Intelligent controller of helicopter turboshaft engines' gas temperature with compensation of transient process's inertial delays and optimization

Serhii Vladov[1], Anatoliy Sachenko[2,3], Nataliia Vladova[4] and Danylo Shved[5]

[1] *Kharkiv National University of Internal Affairs, L. Landau Avenue, 27, Kharkiv, 61080, Ukraine*
[2] *West Ukrainian National University, Lvivska Street, 11, Ternopil, 46009, Ukraine*
[3] *Casimir Pulaski Radom University, Malczewskiego Street, 29, Radom, 26-600, Poland*
[4] *Ukrainian State Flight Academy, Chobanu Stepana Street, 1, Kropyvnytskyi, 25005, Ukraine*
[5] *Lviv Polytechnic National University, Stepan Bandera Street, 12, Lviv, 79013, Ukraine*

Abstract

This research presents the development of an intelligent controller for the helicopter turboshaft engines gas temperature, aimed at compensating for the measuring sensor's inertial delays and optimizing transient processes. The aim is to compensate for inertial delays $\tau \approx 0.025$ seconds and optimize transient processes. The method is based on a double summation circuit with a channel selector, comparing signals from a thermocouple and a gas-generator rotor speed sensor, and an adaptive observer based on Pade approximation and Taylor series expansion provides a prediction of the state at $t + \tau$. The intelligent control law includes a proportional-integral-differential structure with the coefficients γ_i correction via gradient descent. To refine the delay estimate, a two-layer fully connected multilayer perceptron with a SmoothReLU activation function is implemented trained on flight test data was implemented, which reduced τ to 0.016 seconds (−36 %). This module allows to approximate nonlinear relations between input features and the delay value, which ensures the control signal's timely correction and the system's adaptation to changing operating conditions. Modeling of the system in the Matlab Simulink environment demonstrated a significant improvement in the transient process characteristics: overshoot was reduced from 8.0 to 1.5 %, and the mode establishment time was reduced from 4.2 to 3.3 seconds. The neural network module testing showed high predicting accuracy (99.537 % with losses of 0.511 %), confirmed by the determination coefficient R^2 = 0.9717. The neural network use made it possible to reduce the delay value to 0.016 seconds, which corresponds to an improvement of 36 % compared to traditional methods. The obtained results indicate a proposed technique's high potential for improving the helicopter turboshaft engines automatic control system's dynamic accuracy and stability.

Keywords

Automatic control system, gas temperature, transient process, helicopter turboshaft engine, neural network, training, accuracy

1. Introduction

The aviation industry's evolution is closely related to the helicopter's new types of operation (e.g., Eurocopter AS350, Eurocopter EC145, Eurocopter EC225 Super Puma, etc.), characterized by high speed and long range, which requires increasingly sophisticated automation control systems [1, 2]. The manual and automatic control synthesis, as well as the latter rapid development, forced designers to create not only visual devices for humans but also a sensor set, which signals directly affect the automatic system's subsequent links [3]. The most important characteristic of helicopter turboshaft engines (TE) is the gas temperature in front of the compressor turbine, since it significantly determines both the power plant efficiency and its reliability [4, 5]. Thus, these parameters maintaining accurate values is critical to ensuring the helicopter TE's stable operation.

To maintain the set parameters at a fixed throttle position or to change them according to a given law depending on flight conditions and operating modes, the helicopter TE automatic control systems (ACS) are used [6]. The main requirement for modern ACS is compensation for the temperature sensor's inertia so that the measuring devices function without delays [7, 8].

[1]CMIS-2025: Eighth International Workshop on Computer Modeling and Intelligent Systems, May 5, 2025, Zaporizhzhia, Ukraine

serhii.vladov@univd.edu.ua (S. Vladov); as@wunu.edu.ua (A. Sachenko); nataliia.vladova@sfa.org.ua (N. Vladova); danylo.r.shved@lpnu.ua (D. Shved)

0000-0001-8009-5254 (S. Vladov); 0000-0002-0907-3682 (A. Sachenko); 0009-0009-7957-7497 (N. Vladova); 0009-0005-4306-6805 (D. Shved)

The main requirements for helicopter TE ACS include the high static accuracy to maintain a given range (0.3…0.5%), efficiency with a quick response to control (2…3 seconds), and transient processes close to monotonous, which ensures regulation without drops (2…4%) and with a minimum stabilization time [9, 10]. These strict and contradictory conditions cannot be solved by standard methods, which creates the developing complex task of multifunctional automatic control systems for helicopter TE.

2. Related Works

There are known helicopter TE ACS [11–13] that affect a single control parameter, which is the fuel consumption in the combustion chamber, which includes measuring devices for input signals, comparison elements, and an actuator, and the signal from the gas temperature controller directly adjusts the rotor speed controller setting. This scheme's main disadvantage is the reduction in stability reserves and permissible gain factors, which worsens static and dynamic accuracy, and to eliminate this effect, systems with a selector are used, excluding controllers' joint operation area and thereby improving the system's overall characteristics [14, 15]. The helicopter TE gas temperature control system presented in [16] uses a correction link with a differentiator, multiplier blocks, and adders to compensate for the dynamic error caused by the first temperature sensor inertia. The correction coefficient at the derivative changes based on the current gas flow rate signal, which ensures high measurement and control accuracy. However, the scheme's key disadvantage is that in transient modes, the rotor speed and temperature channel's interaction through the selector is not taken into account, which reduces the inertial delay compensation efficiency.

The helicopter TEs gas temperature control using the controller presented in [17] is carried out through correcting devices for the control channels transfer functions changing. This allows for minimizing overshoot and ensuring stable engine operation in various modes. However, its key disadvantage is related to the inertial delays compensation: since the transfer functions correction depends on the velocity pressure, changes in the system occur with a delay, which can cause a temporary mismatch between the required and actual parameters, especially with sharp changes in engine operating modes.

In [18] the engine temperature controller is presented that uses a double summation scheme, in which the measured temperature signal is compared with the set value, and the correction is carried out by a nonlinear element that compensates for the delay in the compressor turbine blades heating. Due to the inertial link, the rotor speed signal is corrected, which eliminates sharp increases in gas temperature in front of the compressor turbine, thereby improving the transient processes quality. As a result, the fuel consumption changes proportionally to the summing amplifier's output signals, ensuring stable and accurate regulation of the engine operation. This controller's main limitation is the long return time to the original mode, due to the isodromic feedback inertia. The intelligent component introduction will allow dynamically optimizing the control parameters and reducing the system response time to changes in operating conditions.

The helicopter TEs intelligent gas temperature controllers integrate modern automatic control methods, including correction links with differentiators, nonlinear elements, and double summation schemes, which allow achieving high accuracy and stability of operation [19, 20]. They ensure overshoot minimization and fast system response, which is critically important for modern helicopters with high-speed and long-range characteristics. However, these systems key disadvantage is insufficient compensation for the measuring sensors inertial delays, which leads to the parameters temporary mismatch in transient modes. Some schemes, for example, [21, 22], aimed at regulating fuel consumption, experience a decrease in stability margins and permissible gain factors, which negatively affects the static and dynamic accuracy of regulation.

3. Goal and Objectives

Thus, a goal of this paper is to develop the helicopter TEs gas temperature intelligent controller, compensating for the measuring sensors inertial delays and optimizing transient processes. To achieve the goal the following objectives are formed: (i) developing the intelligent method for regulating gas temperature, (ii) designing the adaptive algorithms and corrective links with differentiators implementation to control parameters dynamic adjustment for eliminating the time

discrepancy between the required and actual values. Finally, it's expected to increase the system's static and dynamic accuracy and improve its stability, as well as reduce the engine stabilization time.

4. Materials and Methods

4.1. Development of an intelligent gas temperature controller

The proposed controller (Figure 1) is based on a double summation circuit [18]. It is based on a comparative analysis of signals received from thermocouples and a gas-generator rotor speed sensor [23], using an inertial link, a comparison element, and a nonlinear unit for adjusting the fuel supply. This ensures compensation for the delay in heating up the turbine and the temperature regime stabilization. Under normal conditions, the signals from the speed sensor compensate for each other, and when the regime changes abruptly, a correcting pulse appears, leading to a change in fuel consumption proportional to the largest deviation in the summing amplifiers. Under transient conditions, the signal delay through the inertial link leads to the different signal appearance in the comparison element, which is then amplified through the summing devices. The control channel selector selects the largest received deviations, and the nonlinear element with an exponential or parabolic characteristic reduces the specified temperature setting, compensating for the delay in heating up the compressor turbine blades.

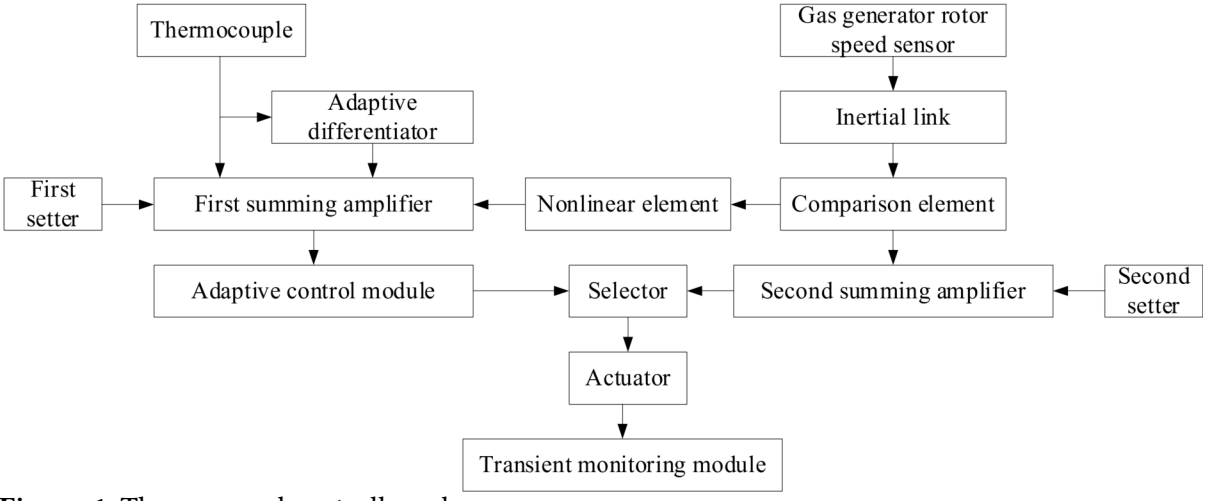

Figure 1: The proposed controller scheme

The proposed scheme for the helicopter TE gas temperature regulating integrates adaptive algorithms and correcting links with differentiators, which allows for dynamic optimization of control parameters and time discrepancies elimination between required and actual values. Adaptive algorithms analyze the transient processes current dynamics and correct the gain factors and inertial links time constants in real time, thus providing a more accurate and timely response to changes in the engine operating mode. The integration of differentiators into measuring circuits allows for predicting trends in temperature conditions, compensating for the delay in turbine warm-up, and a nonlinear element with an exponential characteristic synchronizes system responses, minimizing sharp transient fluctuations. The result is an ACS of adapting to changing operating conditions, increasing the helicopter TE reliability and efficiency.

The proposed controller features include the adaptive control module introduction, which is connected between the summing amplifiers and the control channel selector. This module performs the transmission coefficients real-time correction and the inertial links time constants, responding to the transient processes dynamics and eliminating the time discrepancy between the specified and actual parameters. The adaptive differentiator introduction integrated into the measuring circuit between the thermocouple unit and the first summing amplifier facilitates preliminary signal processing, predicting temperature change trends, and compensating for the delay in heating the compressor turbine blades. The proposed controller also includes a transient mode monitoring unit connected to the actuator to form feedback and dynamically optimize the control algorithms.

Thus, the scientific novelty consists in obtaining further development of the helicopter TE gas temperature controller according to the double summation scheme, which, due to the adaptive

algorithm's introduction integrated with corrective links equipped with differentiators, allows control parameters, real-time optimization, and inertial delays compensation of measuring sensors. This ensures synchronization between the required and actual temperature modes, significantly increasing the helicopter TE accuracy, stability, and efficiency.

4.2. Development of the intelligent method for regulating gas temperature

Based on [17, 18, 23, 24], it is assumed that the gas temperature dynamics is described by the following equation with a delay of the form:

$$\dot{T}(t)=a\cdot T(t)+b\cdot u(t-\tau)+d(t), \tag{1}$$

where $T(t)$ is the gas temperature at time t, $u(t)$ is the control action (for example, change in fuel consumption), a and b are the system coefficients, τ is the measuring inertial delay or actuator links, and $d(t)$ is the external disturbance.

To track the given temperature trajectory $T_{ref}(t)$, we define the control error:

$$e(t) = T_{ref}(t) - T(t). \tag{2}$$

The delayed system transfer function based on the Padé approximation [25] for exponential delay is:

$$e^{-\tau\cdot t}\approx\frac{1-\frac{\tau}{2}\cdot s}{1+\frac{\tau}{2}\cdot s}, \tag{3}$$

from where the system transfer function has the form:

$$G(s)=\frac{b\cdot\left(1-\frac{\tau}{2}\cdot s\right)}{(s-a)\cdot\left(1+\frac{\tau}{2}\cdot s\right)}. \tag{4}$$

To compensate for the measurement delay, an adaptive observer is used that estimates the system state. Let the observer have the form:

$$\hat{\dot{T}}(t)=a\cdot\hat{T}(t)+b\cdot u(t)+K_{obs}\cdot\left(T(t)-\hat{T}(t)\right), \tag{5}$$

where $\hat{T}$ is the temperature estimate and K_{obs} is the observation coefficient (can be chosen as a vector for more complex models, for example, as in [26, 27]).

To compensate for the delay τ, the state prediction at time $t + \tau$ is used using a Taylor series expansion of the form:

$$\hat{T}(t+\tau)=\hat{T}(t)+\tau\cdot\hat{\dot{T}}(t)+\frac{\tau^2}{2}\cdot\hat{\ddot{T}}(t)+\ldots \tag{6}$$

In practical implementation, one can limit oneself to the first or second term of the expansion, as shown, for example, in [16, 18]. To estimate the temperature's second derivative, a difference scheme of the form is used:

$$\hat{\ddot{T}}(t)\approx\frac{T(t)-2\cdot T(t-\Delta t)+T(t-2\cdot\Delta t)}{\Delta t^2}. \tag{7}$$

Based on the adaptive observer mathematical model (5) and the state prediction method (6), an intelligent control law is proposed that takes into account the predicted error:

$$u(t)=k_1(t)\cdot\left(T_{ref}(t)-\hat{T}(t+\tau)\right)+k_2(t)\cdot\dot{T}_{ref}(t)+k_3(t)\cdot\int_0^t\left(T_{ref}(s)-\hat{T}(s+\tau)\right)ds, \tag{8}$$

where $k_1(t)$ is the proportional coefficient, $k_2(t)$ is the differential gain coefficient, $k_3(t)$ is the integral gain coefficient, $\dot{T}_{ref}(t)$ is the given trajectory derivative.

The coefficients $k_i(t)$ are adjusted in real time using adaptive laws, for example, according to the gradient descent scheme:

$$\dot{k}_i(t)=-\gamma_i\cdot e(t)\cdot\phi_i(t), (i = 1, 2, 3, \ldots \tag{9}$$

where $\gamma_i > 0$ are the adaptation rates, $\phi_i(t)$ are the signal functions depending on the system's current state, for example, $\phi_1(t) = T_{ref}(t) - \hat{T}(t+\tau)$, $\phi_2(t) = \dot{T}_{ref}(t)$ and $\phi_2(t) = \int_0^t \left(T_{ref}(s) - \hat{T}(s+\tau)\right) ds$.

To determine the optimal parameters, the quality functional can be minimized:

$$J = \int_t^{t+T_p} \left(Q \cdot \left(T(s) - T_{ref}(s)\right)^2 + R \cdot \left(u(s)\right)^2\right) ds, \tag{10}$$

where $Q, R > 0$ are the weighting coefficients, T_p is the predict horizon.

To improve the compensation accuracy for inertial delays, it is proposed to implement a neural network module [28–30] that corrects the delay estimate:

$$\hat{\tau}(s) = \tau_0 + f_{NN}(\varphi(t)), \tag{11}$$

where τ_0 is the delay base value, $f_{NN}(\bullet)$ is the neural network approximating function, and $\varphi(t)$ is the feature vector (for example, gas generator rotor speed, current temperature dynamics, and other parameters).

Thus, the scientific novelty of the developed intelligent method lies in the adaptive observer with state prediction implementation and a neural network module for compensating for inertial delays, which allows for the control parameters real-time optimization.

Within the developed method framework, theorem 1, "On adaptive stability and convergence of a closed system of intelligent gas temperature control with inertial delays compensation," is formulated. According to the developed intelligent method, the system dynamics is given by the equation $\dot{T}(t) = a \cdot T(t) + b \cdot u(t-\tau) + d(t)$ provided that the disturbances $d(t)$ are bounded and the adaptive observer has the form $\dot{\hat{T}}(t) = a \cdot \hat{T}(t) + b \cdot u(t) + K_{obs} \cdot \left(T(t) - \hat{T}(t)\right)$, in this case, the control action is determined by the law $u(t) = k_1(t) \cdot \left(T_{ref}(t) - \hat{T}(t+\tau)\right) + k_2(t) \cdot \dot{T}_{ref}(t) + k_3(t) \cdot \int_0^t$ ¿¿ $- \hat{T}(s+\tau)\big) ds$, and the adaptive coefficients change as $\dot{k}_i(t) = -\gamma_i \cdot e(t) \cdot \phi_i(t)$, ($i$ = 1, 2, 3, ...). If there exists a Lyapunov function of the form $V(t) = \frac{1}{2} \cdot \left(e(t)\right)^2 + \sum_{i=1}^{3} \frac{1}{2 \cdot \gamma_i} \cdot \left(k_i(t) - k_i^{¿}(t)\right)^2$, where $k_i^{¿}$ are the coefficient's optimal values, and if for some α, $\beta > 0$ the inequality holds $\dot{V}(t) \le \alpha \cdot V(t) + \beta \cdot \left\|d(t)\right\|^2$, then the closed system is uniformly bounded in finite time, and the tracking error $e(t) = T_{ref}(t) - T(t)$ asymptotically tends to an arbitrarily small neighborhood of zero, provided that the perturbations $d(t)$ are sufficiently small.

Proof of Theorem 1.

Let us consider a candidate for a Lyapunov function of the form

$$V(t) = \frac{1}{2} \cdot \left(e(t)\right)^2 + \sum_{i=1}^{3} \frac{1}{2 \cdot \gamma_i} \cdot \left(\tilde{k}_i(t)\right)^2, \tag{12}$$

where

$$e(t) = T_{ref}(t) - T(t),\ \tilde{k}_i(t) = k_i(t) - k_i^{¿}(t)\ (i = 1, 2, 3, \ldots), \tag{13}$$

and $k_i^{¿}$ are the coefficient's optimal (constant) values, and $\gamma_i > 0$ are the adaptation constants.

Differentiate $V(t)$ with respect to time:

$$\dot{V}(t) = e(t) \cdot \dot{e}(t) + \sum_{i=1}^{3} \frac{1}{\gamma_i} \cdot \tilde{k}_i(t) \cdot \dot{\tilde{k}}_i(t), \tag{14}$$

Since $k_i^{¿}$ are constant, then $\dot{k}_i^{¿}(t) = \dot{k}_i^{¿}$. Taking into account the adaptation law (9), we obtain:

$$\dot{V}(t) = e(t) \cdot \dot{e}(t) - \sum_{i=1}^{3} \tilde{k}_i(t) \cdot e(t) \cdot \phi_i(t). \tag{15}$$

Since the gas temperature dynamics is given by equation (1), and the control action is selected according to the law (8) using the adaptive observer (5) and under the correct delay compensation

condition (using the state prediction according to the Taylor series) (6), it can be shown that the error dynamics $e(t) = T_{ref}(t) - T(t)$ in a closed system approximately takes the form

$$\dot{e}(t) = -\sum_{i=1}^{3} k_i^{\cdot} \cdot e(t) + \delta(t), \tag{16}$$

where $\delta(t)$ combines model errors, delay compensation and external disturbances, and $\phi_i(t)$ are signal functions that depend on the system's state.

When substituting (16) into (15) we obtain:

$$\dot{V}(t) = e(t) \cdot \left(-\sum_{i=1}^{3} k_i^{\cdot} \cdot e(t) + \delta(t) \right) - \sum_{i=1}^{3} \tilde{k}_i(t) \cdot e(t) \cdot \phi_i(t). \tag{17}$$

Let's group the terms:

$$\dot{V}(t) = -(e(t))^2 \cdot \sum_{i=1}^{3} k_i^{\cdot} \cdot \phi_i(t) - e(t) \cdot \sum_{i=1}^{3} \tilde{k}_i(t) \cdot \phi_i(t) + e(t) \cdot \delta(t). \tag{18}$$

Note that

$$\sum_{i=1}^{3} \left(k_i^{\cdot} + \tilde{k}_i(t) \right) \cdot \phi_i(t) = \sum_{i=1}^{3} k_i(t) \cdot \phi_i(t), \tag{19}$$

and with the $\phi_i(t)$ and $k_i(t)$ correct choice it is assumed that the total term $\sum_{i=1}^{3} k_i(t) \cdot \phi_i(t)$ is a positive definite function, that is, there exists $\lambda > 0$ such that

$$\sum_{i=1}^{3} k_i(t) \cdot \phi_i(t) \geq \lambda > 0. \tag{20}$$

Thus, the assessment can be written as:

$$\dot{V}(t) = -\lambda \cdot (e(t))^2 + e(t) \cdot \delta(t). \tag{21}$$

We use Yong's inequality:

$$e(t) \cdot \delta(t) \leq \frac{\lambda}{2} \cdot (e(t))^2 + \frac{1}{2 \cdot \lambda} \cdot (\delta(t))^2. \tag{22}$$

Hence,

$$\dot{V}(t) \leq -\lambda \cdot (e(t))^2 + \frac{\lambda}{2} \cdot (e(t))^2 + \frac{1}{2 \cdot \lambda} \cdot (\delta(t))^2 = \frac{-\lambda}{2} \cdot (e(t))^2 + \frac{1}{2 \cdot \lambda} \cdot (\delta(t))^2. \tag{23}$$

Taking into account that the function $V(t)$ satisfies the inequality

$$V(t) \geq \frac{1}{2} \cdot (e(t))^2, \tag{24}$$

the final assessment was received:

$$\dot{V}(t) \leq -\lambda \cdot V(t) + \frac{1}{2 \cdot \lambda} \cdot (\delta(t))^2. \tag{25}$$

Denoting $\alpha = \lambda$ and $\beta = \frac{1}{2 \cdot \lambda}$, then

$$\dot{V}(t) \leq -\alpha \cdot V(t) + \beta \cdot \|\delta(t)\|^2. \tag{26}$$

According to the comparison lemma, if $\dot{V}(t) \leq -\alpha \cdot V(t) + \beta \cdot \|\delta(t)\|^2$, then the function $V(t)$ has the uniform finite boundedness property, that is, there exists a constant V_∞ such that

$$\limsup_{t \to \infty} V(t) \leq \frac{\beta}{\alpha} \cdot^{\cdot} t \geq 0 \|\delta(t)\|^2. \tag{27}$$

Since $V(t)$ includes the term $\frac{1}{2} \cdot \left(e(t)\right)^2$, this means that the error $e(t)$ asymptotically approaches a zero neighborhood whose size is determined by the quantity $¿_{t \geq 0} \left\|\delta(t)\right\|$. Provided that the disturbances and delay compensation errors are sufficiently small, this neighborhood can be made arbitrarily small.

Thus, it is proved that the closed system with the chosen adaptive control law and the coefficient adaptation law is uniformly finitely determined, and the tracking error $e(t) = T_{ref}(t) - T(t)$ asymptotically tends to an arbitrarily small neighborhood of zero. This means

$$\dot{V}(t) \leq -\alpha \cdot V(t) + \beta \cdot \left\|\delta(t)\right\|^2 \Rightarrow \limsup_{t \to \infty} V(t) \leq \frac{\beta}{\alpha} \cdot ¿ t \geq 0 \left\|\delta(t)\right\|^2,$$

which proves the theorem on adaptive stability and convergence.

4.3. Development of a neural network module for delay estimation correction

Based on [31–33], we propose to use a deep fully connected (feedforward) neural network to approximate the function $f_{NN}(\varphi(t))$ (Figure 2). The neural network architecture is defined by an input layer of dimension n, where $\varphi(t) \in \mathbb{R}^n$, followed by one or more hidden layers with nonlinear activation functions; in particular, for the two-layer MLP architecture example [34], the first hidden layer contains m_1 neurons, and the second contains m_2 neurons, after which the output layer, consisting of one neuron with linear activation, forms the correction value.

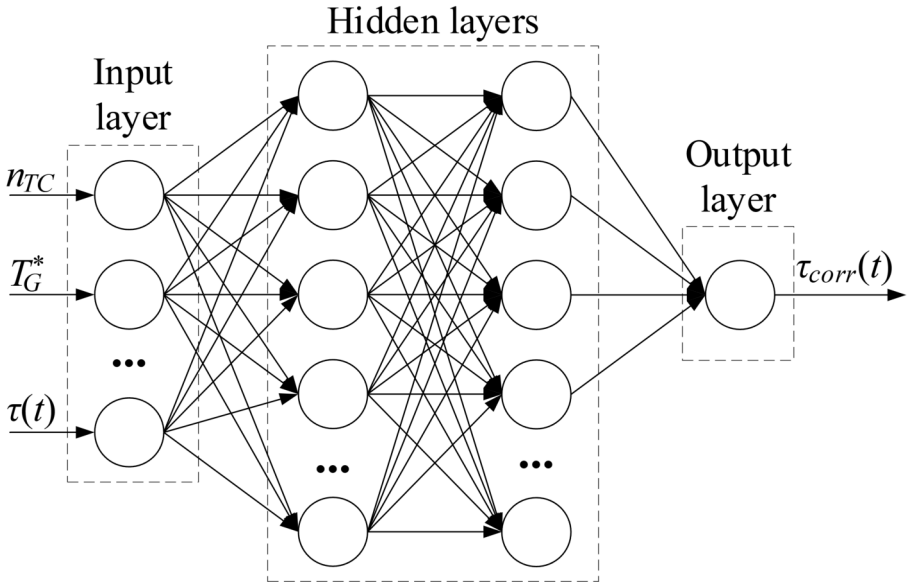

Figure 2: Architecture of the proposed deep fully connected (feedforward) neural network

In the general case, for a neural network with L layers (excluding the input), the input is initialized as $a^{(0)} = \varphi(t)$. For each hidden layer $l = 1, \ldots, L - 1$, the calculation is performed:

$$z^{(l)} = W^{(l)} \cdot a^{(l-1)} + b^{(l)}, \tag{28}$$

$$a^{(l)} = \sigma^{(l)} \cdot \left(z^{(l)}\right), \tag{29}$$

where $W^{(l)}$ is the weight matrix, $b^{(l)}$ is the bias vector, and $\sigma^{(l)}(\bullet)$ is the activation function (e.g. ReLU, SmoothReLU [35], tanh, or sigmoid).

At the output layer ($l = L$) the following is calculated:

$$z^{(l)} = W^{(L)} \cdot a^{(L-1)} + b^{(L)}, \tag{30}$$

$$f_{NN}\left(\varphi(t)\right) = W^{(L)} \cdot a^{(L)} = z^{(L)}, \tag{31}$$

where a linear activation function is used since the problem is a regression problem.

Thus, the delay adjustment module has the form:

$$\tau_{corr}(t) = \tau_0 + z^{(L)}. \tag{32}$$

In this research, we propose the neural network architecture with two hidden layers use (Figure 2), for which the presented expressions will have the form presented in Table 1.

Table 1

Basic analytical expressions for the applied neural network

Number	Layer	Analytical expression
1	First hidden layer (l = 1)	$z^{(1)} = W^{(1)} \cdot \varphi(t) + b^{(1)}, a^{(1)} = Smooth\,ReLU^{(1)}\left(z^{(1)}\right)$
2	Second hidden layer (l = 2)	$z^{(2)} = W^{(2)} \cdot a^{(1)} + b^{(2)}, a^{(2)} = Smooth\,ReLU^{(2)}\left(z^{(2)}\right)$
3	Output layer (l = 3)	$z^{(3)} = W^{(3)} \cdot a^{(2)} + b^{(3)}, f_{NN}(\varphi(t)) = z^{(3)}$
4	Final delay estimate	$\tau_{corr}(t) = \tau_0 + z^{(3)}$

To determine the parameters $\Theta = \left\{W^{(l)}, b^{(l)}\right\}_{l=1}^{L}$, the neural network is trained on historical data, where for each time moment t_i the feature vector $\varphi(t_i)$ and the actual delay τactual(t_i) are known. The training task is to minimize the loss function, for example, the mean square error (MSE), as shown in [36, 37]:

$$L(\Theta) = \frac{1}{2 \cdot N} \cdot \sum_{i=1}^{N} \left(\tau_{actual}(t_i) - \left(\tau_0 + f_{NN}(\varphi(t_i))\right)\right)^2 + \lambda \cdot \sum_{l=1}^{L} \left(W^{(l)}\right)_2^2, \quad (33)$$

where $\lambda > 0$ is the regularization coefficient [36].

The neural network parameters are updated according to the gradient descent rule:

$$\Theta \leftarrow \Theta - \eta \cdot \nabla_{\Theta} L(\Theta), \quad (34)$$

where $\eta > 0$ is the training rate.

At the same time, gradients are calculated at each layer using backpropagation. For example, for the last layer, the error at the output layer is calculated as:

$$\delta^{(L)} = \frac{\partial L}{\partial z^{(L)}} = a^{(L)} - \left(\tau_{actual} - \tau_0\right). \quad (35)$$

For each previous layer $l = L - 1, L - 2, \ldots, 1$ the following is determined:

$$\delta^{(l)} = W^{(l+1)T} \odot \sigma'^{(l)}\left(z^{(l)}\right), \quad (36)$$

where $\odot$ denotes element-wise multiplication and $\sigma'^{(l)}$ is the activation function derivative.

The weights and biases update for the l-th layer is performed as:

$$W^{(l)} = W^{(l)} - \eta \cdot \delta^{(l)}\left(a^{(l-1)}\right)^T, \quad (37)$$

$$b^{(l)} = b^{(l)} - \eta \cdot \delta^{(l)}. \quad (38)$$

The resulting delay estimate $\tau_{corr}(t)$ is used to correct the control action in the control scheme. If the control law (8) was previously written as

$$u(t) = k_1(t) \cdot e(t) + k_2(t) \cdot \dot{e}(t) + k_3(t) \cdot \int e(t)\,dt, \quad (39)$$

then, taking into account the delay correction, it can be supplemented as follows. For example, the parameter $\tau_{corr}(t)$ can be taken into account when predicting the state through the expansion in a Taylor series:

$$\hat{T}\left(t + \tau_{corr}(t)\right) = \hat{T}(t) + \tau_{corr}(t) \cdot \hat{\dot{T}}(t) + \frac{1}{2} \cdot \hat{\ddot{T}}(t) \cdot \left(\tau_{corr}(t)\right)^2 + \ldots \quad (40)$$

Thus, the neural network module for correcting the delay estimate is implemented according to the scheme $\tau_{corr}(t) = \tau_0 + f_{NN}(\varphi(t))$, where the function $f_{NN}(\varphi(t))$ is approximated by a neural network constructed according to the scheme (27)–(32). The module is trained by minimizing MSE (33) with updating the parameters according to (34)–(38). When integrated into the general control algorithm, the $\tau_{corr}(t)$ value is used to accurately predict the system state (20), which significantly improves the control quality in the inertial delays presence.

5. Case study

5.1. Results of the helicopter turboshaft engine gas temperature control channel with the two value's algebraic minimum selector research

It is accepted that, in general, the proposed intelligent gas temperature controller (Figure 3) is a two-channel controller: the gas temperature in front of the compressor turbine regulating channel and the gas generator rotor speed regulating channel [23, 38] (the free turbine rotor speed regulating channel [39] is not taken into account).

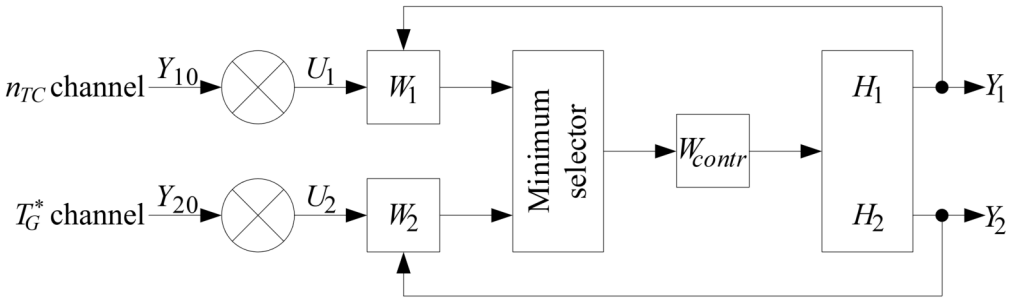

Figure 3: Proposed intelligent controller circuit

According to Figure 3, the minimum selector is described by the expression:

$$U=\begin{cases}U_1, U_1 \le U_2,\\ U_2, U_1 > U_2,\end{cases} \tag{41}$$

where H_1 is the object's (engine TV3-117) transfer function in the first control channel (the gas generator rotor speed channel) $H_1=\frac{1}{T\cdot s}$, H_2 is the object's (engine TV3-117) transfer function in the second channel (the gas temperature in front of the compressor turbine channel) $H_2 = 1$, where:

$$W_{contr}=\frac{k_{contr}}{s\cdot(\tau\cdot s+1)},\ W_1 = k_1,\ W_2 = k_2, \tag{42}$$

where Y_{10} and Y_{20} are constant settings.

Let's consider the individual open channel's transfer functions:

$$W_I(s)=\frac{k_1\cdot k_{contr}}{s\cdot(T\cdot s+1)\cdot(\tau\cdot s+1)}, \tag{43}$$

$$W_I(j\omega)=\frac{k_1\cdot k_{contr}}{j\omega\cdot(T\cdot j\omega+1)\cdot(\tau\cdot j\omega+1)}=\frac{k_1\cdot k_{contr}}{-(\tau+T)\cdot\omega^2+j\omega\cdot(1-\tau\cdot T\cdot\omega^2)}=¿$$
$$¿\frac{k_1\cdot k_{contr}\cdot(\tau+T)^2\cdot\omega^4}{(\tau+T)\cdot\omega^4+\omega^2\cdot(1-\tau\cdot T\cdot\omega^2)^2}-j\cdot\frac{k_1\cdot k_{contr}\cdot(1-\tau\cdot T\cdot\omega^2)}{(\tau+T)\cdot\omega^4+\omega^2\cdot(1-\tau\cdot T\cdot\omega^2)^2}, \tag{44}$$

$$W_I(s)=\frac{k_2\cdot k_{contr}}{s\cdot(\tau\cdot s+1)}, \tag{45}$$

$$W_{II}(j\omega)=\frac{k_2\cdot k_{contr}}{-\tau\cdot\omega^2+j\omega}=\frac{k_2\cdot k_{contr}\cdot\tau\cdot\omega^2}{\tau^2\cdot\omega^4+\omega^2}-j\cdot\frac{k_2\cdot k_{contr}\cdot\omega}{\tau^2\cdot\omega^4+\omega^2}, \tag{46}$$

where $k_1 = 10$, $k_2 = 1$, $k_p = 10$, $T = 0.5$ second, $\tau = 0.025$ second [37, 38].

Then the proposed two-channel intelligent controller's transfer function will have the form:

$$\Phi(s)=\frac{W_I(s)-W_{II}(s)}{2+W_I(s)+W_{II}(s)}=\frac{k_1\cdot k_{contr}-k_2\cdot k_{contr}\cdot(T\cdot s+1)}{2\cdot(T\cdot s+1)\cdot(T\cdot s+1)\cdot s+k_1\cdot k_{contr}+k_2\cdot k_{contr}\cdot(T\cdot s+1)} \tag{47}$$

$$\Phi(j\omega)=\frac{\left(k_1\cdot k_{contr}-k_2\cdot k_{contr}\right)-j\cdot k_2\cdot k_{contr}\cdot T\cdot\omega}{k_1\cdot k_{contr}-k_2\cdot k_{contr}-2\cdot k_2\cdot k_{contr}\cdot T\cdot\omega^2+j\cdot\left(\left(2+k_2\cdot k_{contr}\cdot T\right)\cdot\omega-2\cdot T\cdot\tau\cdot\omega^3\right)}=$$

$$=\frac{\left(k_1\cdot k_{contr}-k_2\cdot k_{contr}\right)-k_2\cdot k_{contr}\cdot T\cdot\omega}{\left(k_1\cdot k_{contr}-k_2\cdot k_{contr}-2\cdot k_2\cdot k_{contr}\cdot T\cdot\omega^2\right)^2+\left(\left(2+k_2\cdot k_{contr}\cdot T\right)\cdot\omega-2\cdot T\cdot\tau\cdot\omega^3\right)^2}- \quad (48)$$

$$-j\cdot\frac{\left(k_1\cdot k_{contr}-k_2\cdot k_{contr}\right)\cdot\left(\left(2+k_2\cdot k_{contr}\cdot T\right)\cdot\omega-2\cdot T\cdot\tau\cdot\omega^3\right)+k_2\cdot k_{contr}\cdot T\cdot\omega\cdot\left(k_1\cdot k_{contr}-k_2\cdot k_{contr}-2\cdot k_2\cdot k_{contr}\cdot T\cdot\omega^2\right.}{\left(k_1\cdot k_{contr}-k_2\cdot k_{contr}-2\cdot k_2\cdot k_{contr}\cdot T\cdot\omega^2\right)^2+\left(\left(2+k_2\cdot k_{contr}\cdot T\right)\cdot\omega-2\cdot T\cdot\tau\cdot\omega^3\right)^2}$$

The Nyquist hodographs constructed for the system's individual loops with the values $k_1 = 10$, $k_2 = 1$, $k_{contr} = 10$, $T = 0.5$ second, $\tau = 0.025$ second [23, 38] demonstrate that in this automatic control system with a minimum selector, the closed loop $W_{\text{I}}(s)$ is unstable, while the closed loop $W_{\text{II}}(s)$ is stable (Figure 4).

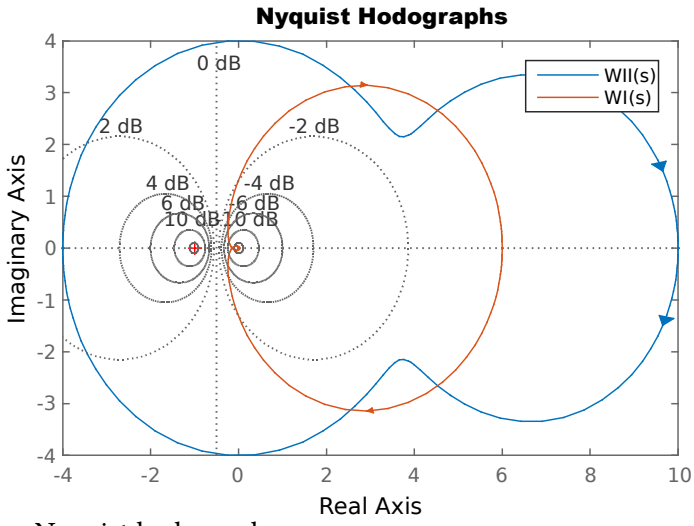

Figure 4: The resulting Nyquist hodographs

The transformed system's $\Phi(s)$ linear link amplitude-phase characteristic is shown in Figure 5. The condition for the oscillation's occurrence in such a nonlinear system is the equivalent linear part's $\Phi(s)$ hodograph's intersection point with the complex nonlinearity coefficient's hodograph. In this case, the latter corresponds to the negative segment of the real axis in the range from −1 to −∞. It follows from this those oscillations with a frequency of $\omega \approx 12.227$ s^{-1} ($f \approx 1.96$ Hz) can occur in this system.

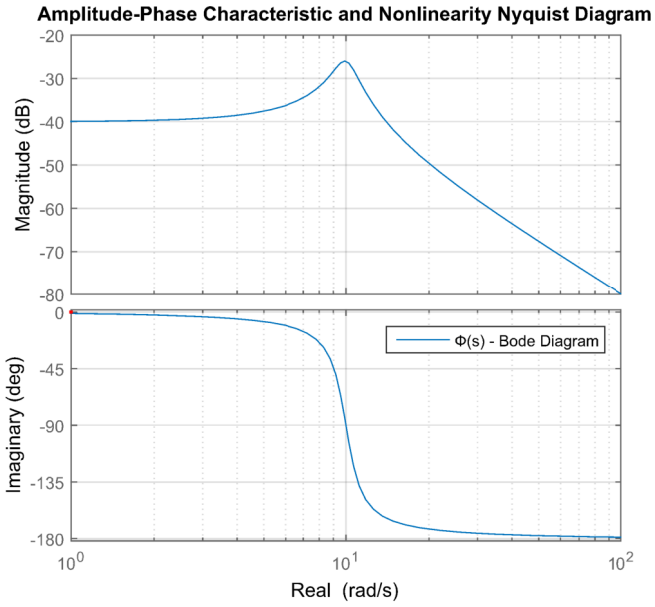

Figure 5: The transformed system's linear link's resulting amplitude-phase characteristic

In this research, the system's behavior in the time domain was analyzed. For this aim, the controller links were presented using differential equations:

$$W(s)=\frac{1}{\tau\cdot s+1}=\frac{U_{out}}{U_{¿}},\ U_{¿}(s)=T\cdot\frac{dU_{out}(s)}{dt}+U_{out}(s),\ \text{or}$$

$$\frac{dU_{out}(s)}{dt}=\frac{1}{T}\cdot U_{¿}-\frac{1}{T}\cdot U_{out}, \tag{49}$$

$$W(s)=\frac{k_{contr}}{s\cdot(\tau\cdot s+1)}=\frac{U_{out}}{U_{¿}},\ \tau\cdot\frac{d^2U_{out}(s)}{dt^2}+\frac{dU_{out}(s)}{dt}=k_{contr}\cdot U_{¿}.$$

Therefore, this system is characterized by two differential equations set and an equation that determines the selector switching:

$$\begin{cases}\dfrac{dx}{dt}=\dfrac{Z}{T}-\dfrac{x}{T},\\ \tau\cdot\dfrac{d^2Z}{dt^2}+\dfrac{dZ}{dt}=k_{contr}\cdot U,\end{cases} \tag{50}$$

$$U=\begin{cases}U_1, U_1-U_2\le 0,\\ U_2, U_1-U_2>0.\end{cases} \tag{51}$$

The system remains stable when the condition is met: $Y_{10} = 1$, $Y_{20} < 1$ (if $Y_{20} > 1$, oscillations occur). In this region, the output variables change exponentially. The second circuit is closed (Figure 3), and Y_2 reaches the steady-state value in $t_{contr} = 0.25...0.3$ seconds. At the setpoint value $Y_{20} > 1$, oscillations occur in the system that do not damp. Their frequency remains unchanged and is $f \approx 1.96$ Hz; $T = 0.427$ seconds. The oscillation's amplitude increases as the setpoint increases.

To eliminate temperature overload, corrective elements are introduced [40]. The selection condition is determined by the following expression [40, 41]:

$$U_{n_{TC}}=U_{T_G^{¿}}. \tag{52}$$

In this research, two selection options were considered, similar to [41]:

$$\varepsilon_2 = Y_{20} - Y_2 = 0, \tag{53}$$

$$\varepsilon_1 = \varepsilon_2. \tag{54}$$

In this research, the correcting link's $W_{k1}(s)$ and $W_{k2}(s)$ transfer functions are determined based on the selection conditions. For the first condition (53):

$$U_{n_{TC}}=W_{n_{TC}}(s)\cdot\varepsilon_1, \tag{55}$$

$$U_{T_G^{¿}}=W_{T_G^{¿}}(s)+W_{k1}(s)\cdot W_{T_G^{¿}}(s)\cdot s+W_{k2}(s)\cdot W_{T_G^{¿}}(s)\cdot\varepsilon_2. \tag{56}$$

From the selection condition (52):

$$W_{n_{TC}}(s)\cdot\varepsilon_1-W_{T_G^{¿}}(s)+W_{k1}(s)\cdot W_{T_G^{¿}}(s)\cdot s+W_{k2}(s)\cdot W_{T_G^{¿}}(s)\cdot\varepsilon_2, \tag{57}$$

if

$$W_{n_{TC}}(s)=W_{k1}(s)\cdot W_{T_G^{¿}}(s), \tag{58}$$

and

$$W_{T_G^{¿}}(s)+W_{k1}(s)\cdot W_{T_G^{¿}}(s)=1, \tag{59}$$

then $\varepsilon_2 = 0$.

Then

$$W_{k1}(s)=\frac{W_{n_{TC}}(s)}{W_{T_G^{¿}}(s)}, \tag{60}$$

$$W_{k2}(s)=\frac{1-W_{T_G^{¿}}(s)}{W_{T_G^{¿}}(s)}, \tag{61}$$

For the second condition (54) expressions (55) – (57) are valid and if

$$W_{n_{TC}}(s)-W_{k1}(s)\cdot W_{T_G^i}(s)=1, \tag{62}$$

$$W_{T_G^i}(s)-W_{k2}(s)\cdot W_{T_G^i}(s)=1, \tag{63}$$

$$W_{k1}(s)=\frac{W_{n_{TC}}(s)-1}{W_{T_G^i}(s)}, \tag{64}$$

$$W_{k2}(s)=\frac{1-W_{T_G^i}(s)}{W_{T_G^i}(s)}. \tag{65}$$

For modeling and calculations in this study, the parameters of the TV3-117 engine, which is the Mi-8MTV helicopter's power plant's part, were used [42]:

$$(0.21\cdot s+1)\cdot x_{n_{TC}}=(0.229\cdot s+1.306)\cdot x_{G_T}, \tag{66}$$

$$(0.064\cdot s^2+0.667\cdot s+1)\cdot x_{T_G^i}=(0.522\cdot s+3)\cdot x_{G_T}, \tag{67}$$

where $x_{n_{TC}}$ is the output signal for the turbocharger rotor speed, $x_{T_G^i}$ is the output signal for the gas temperature in front of the compressor turbine, x_{G_T} is the input signal for fuel consumption.

From (66), (67) the gas generator rotor speed $W_{n_{TC}}^{G_T}$ and the gas temperature in front of the compressor turbine $W_{T_G^i}^{G_T}$ transfer functions are obtained, identical to those in [38]:

$$W_{n_{TC}}^{G_T}(s)=\frac{0.229\cdot s+1.306}{0.21\cdot s+1}, \tag{68}$$

$$W_{T_G^i}^{G_T}(s)=\frac{0.522\cdot s+3}{0.064\cdot s^2+0.667\cdot s+1}. \tag{69}$$

From (67) and (68) it follows that the gas generator rotor speed controllers $W_{n_{TC}}(s)$ and the gas temperature in front of the compressor turbine $W_{T_G^i}(s)$ transfer functions have the form:

$$W_{n_{TC}}(s)=\frac{1}{0.229\cdot s+1.306}, \tag{70}$$

$$W_{T_G^i}(s)=\frac{1}{0.522\cdot s+3}. \tag{71}$$

Then, according to (60), (61), (64), (65), the first and second correction links $W_{k1}(s)$ and $W_{k2}(s)$ transfer functions are obtained, respectively, for conditions (53) (*I*) and (54) (*II*):

$$W_{k1}^{(I)}(s)=\frac{0.522\cdot s+3}{0.229\cdot s+1.306}, \tag{72}$$

$$W_{k2}^{(I)}(s)=0.522\cdot s+2, \tag{73}$$

$$W_{k1}^{(II)}(s)=\frac{0.12\cdot s^2+0.847\cdot s+0.918}{0.229\cdot s+1.306}, \tag{74}$$

$$W_{k2}^{(I)}(s)=0.522\cdot s+2. \tag{75}$$

It is noted that in [38], the analytical expressions describing the first and second correcting links $W_{k1}(s)$ and $W_{k2}(s)$ transfer functions have the form:

$$W_{k1}(s)=\frac{(-0.0018\cdot s+0.0517)\cdot(0.064\cdot s^2+0.667\cdot s+1)}{0.036\cdot s^2+0.38\cdot s+1}, \tag{76}$$

$$W_{k2}(s)=\frac{0.021\cdot s^2+0.048\cdot s-2}{0.174\cdot s+1}. \tag{77}$$

Thus, in the refined transfer functions $W_{k1}(s)$ and $W_{k2}(s)$ (72)–(75) compared to (76)–(77), a decrease in the variable s orders is observed, which allows eliminating high-order terms that increase the

system's dynamic sensitivity. In this case, only those terms are preserved that to the greatest extent determine the phase and amplitude characteristics necessary to compensate for inertial delays. The analysis shows that the dominant low-order terms (e.g., constant and linear in s) provide adequate delay suppression and maintenance of the required transient process, minimizing overshoot and stabilizing the ACS. This approach simplifies the correcting link's model, reduces the computational load and reduces the high-frequency noise amplification, which significantly increases the adaptability and reliability of the helicopter TE control system.

5.2. Modeling of the TV3-117 engine's gas temperature in front of the compressor turbine controller

According to Figure 3, the Matlab Simulink 2014b software package has constructed simulation schemes in two versions: without correction links (Figure 6a) and with correction links (Figure 6b). The simulation results are shown in Figure 7. It is noted that the actuator's (isodromic controller's) transfer function is adopted, according to [38], in the form:

$$W_{IC}(s)=\frac{3\cdot(0.56\cdot s+1)}{s\cdot(0.02\cdot s+1)}=\frac{1.68\cdot s+3}{0.02\cdot s^2+s}. \quad (78)$$

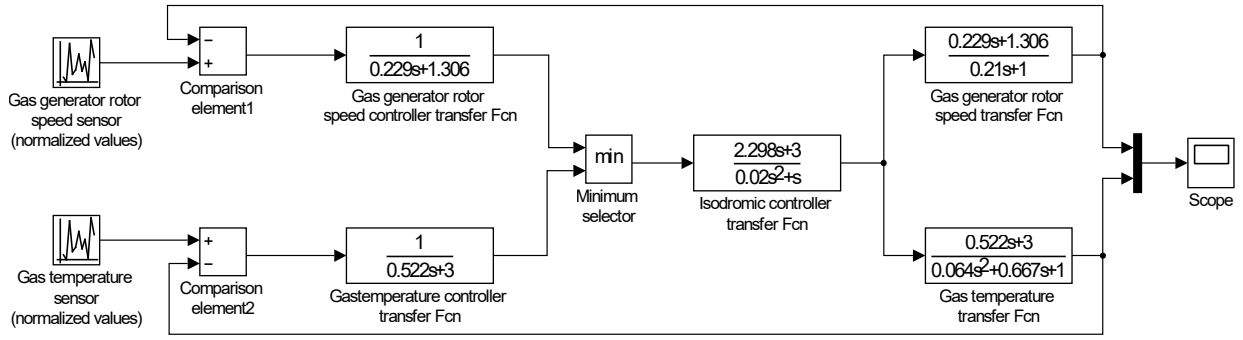

a

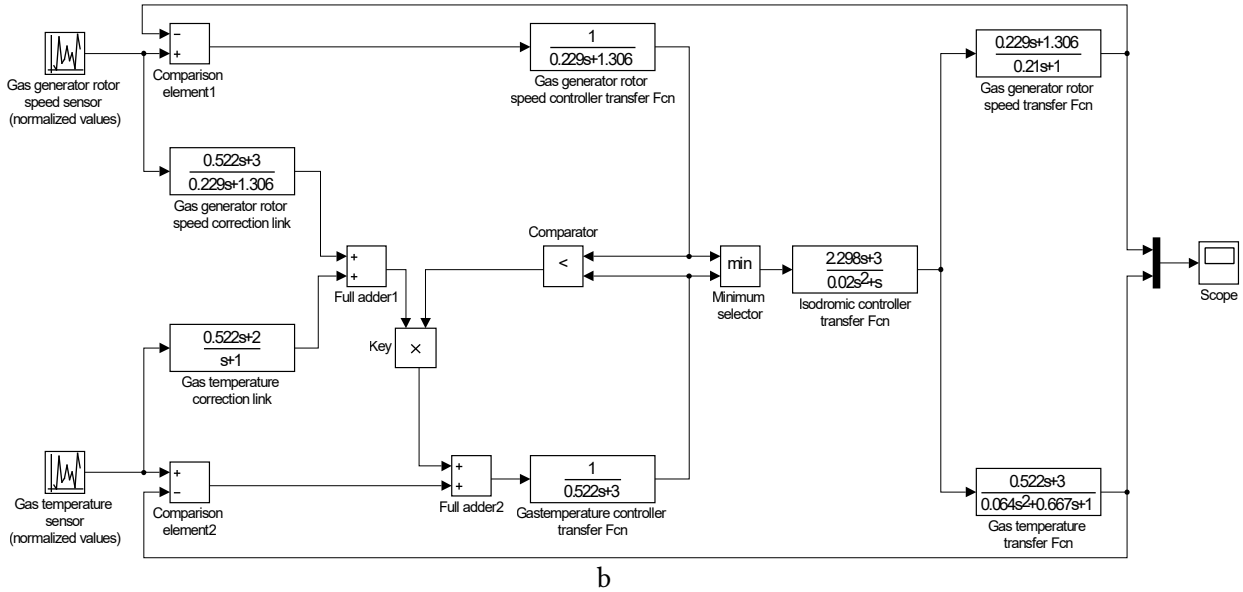

b

Figure 6: Developed schemes for modeling the gas temperature in front of the compressor turbine controller: (a) without correcting links; (b) with correcting links

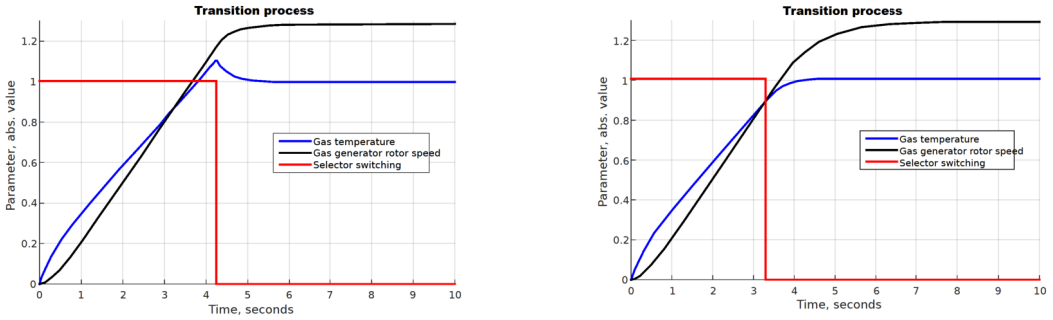

a b

Figure 7: Resulting transient processes diagrams: (a) without correcting links; (b) with correcting links

In Figure 7, the blue curve corresponds to the gas temperature in front of the compressor turbine control channel, the black curve corresponds to the gas generator rotor speed control channel, and the red curve corresponds to the selector switching moment. The first diagram (Figure 7a) illustrates the transient process before the correction link's application: since the gas temperature in front of the compressor turbine controller has inertia with respect to the gas generator rotor speed controller, the selector switches with a delay, which leads to a temporary surge in the gas temperature transmission. To improve the dynamic accuracy of the system when changing the selector, it is necessary to introduce correction links, which is demonstrated in Figure 7b, where more efficient selection and the gas temperature channel connection is ensured, excluding the specified temperature mode excess. The transient processes qualitative characteristic's parameters can be quantitatively described as follows:

- The transient process's time interval (t_{trans}), reflecting the system's response speed and defined as the time interval from the dynamic changes beginning to the moment when the difference between the output signal and its new steady-state level becomes less than 5 % (for the first diagram (Figure 7a) t_{trans1} = 4.2 seconds, and for the second (Figure 7b) t_{trans2} = 3.3 seconds;
- Maximum excess in the transition period σ (overshoot), which is equal to:

$$\sigma = \frac{h(t)_{\text{setting}}(t)_{max}}{h_{\text{setting}}(t)} \tag{79}$$

For the first diagram (Figure 7a) $\sigma_1 = \frac{1.08-1}{1} \cdot 100\,\% = 8\,\%$. For the second diagram (Figure 7b) $\sigma_2 = \frac{1.015-1}{1} \cdot 100\,\% = 1.5\,\%$. Thus, the correction links with transfer functions (72)–(75) introduction makes it possible to virtually eliminate overshoot in the helicopter TE gas temperature in front of the compressor turbine control channel (the overshoot value does not exceed 1.5 %).

5.3. Test results of the neural network module for adjusting the delay estimation

During the research it was established that oscillations with a frequency of $f \approx 1.96$ Hz (the delay is 0.025 seconds) can occur in the developed controller. Therefore, it is advisable to conduct a delay dynamic's research in this frequency vicinity. For this aim, the Mi-8MTV helicopter flight tests results, the power plant of which consists of two TV3-117 engines [42], are used (the data for the left engine are used in the research). In response to an official request sent by the authors to the Ministry of Internal Affairs of Ukraine, information was obtained on the gas temperature in front of the compressor turbine (T_G^i) and the gas generator rotor speed (n_{TC}) in the nominal engine operating mode. The request was fulfilled within the research project "Theoretical and Applied Aspects of Aviation Sphere Development" (number 0123U104884) framework. The data was obtained based on the Mi-8MTV helicopter's flight tests. The experiments were conducted at an altitude of 2500 meters above sea level. The test duration was 320 seconds. The sampling step was 0.25 seconds.

The n_{TC} and T_G^i data obtained during the Mi-8MTV helicopter's flight tests using the onboard monitoring system were preliminarily cleared of noise interference and abnormal emissions. After that, they were transformed into time series are the parameter's sequences ordered by time [43]. To ensure the time series with different scales comparability, the z-normalization procedure was applied:

$$z\left(n_{TC}\right)_i=\frac{n_{TC}^{(i)}-\frac{1}{N}\cdot\sum_{i=1}^{N}n_{TC}^{(i)}}{\sqrt{\frac{1}{N}\cdot\sum_{i=1}^{N}\left(n_{TC}^{(i)}-\sum_{i=1}^{N}n_{TC}^{(i)}\right)^2}},\ z\left(T_G^{¿}\right)_i=\frac{T_G^{¿(i)}-\frac{1}{N}\cdot\sum_{i=1}^{N}T_G^{¿(i)}}{\sqrt{\frac{1}{N}\cdot\sum_{i=1}^{N}\left(T_G^{¿(i)}-\sum_{i=1}^{N}T_G^{¿(i)}\right)^2}},\quad(80)$$

where $N = 1280$.

Thus, the parameters n_{TC} and $T_G^{¿}$ resulting dynamic diagrams after data normalization have the form shown in Figure 8.

The n_{TC} and $T_G^{¿}$ normalized values formed the training dataset, which fragment is presented in Table 2. It is noted that the dataset is homogeneous according to the Fisher-Pearson [44, 45] and Fisher-Snedecor [46, 47] criteria (the homogeneity assessment results are presented in Table 3).

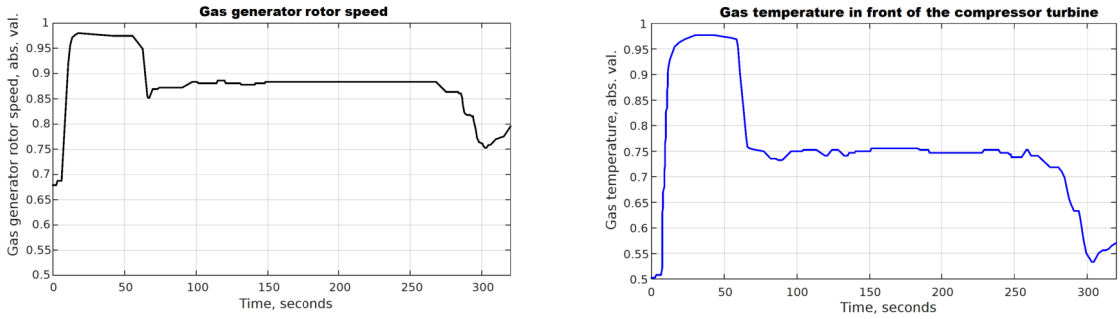

a b

Figure 8: Dynamic diagrams of the TV3-117 engine's gas generator rotor speed (a) and gas temperature in front of the compressor turbine (b)

Table 2
Training dataset fragment

Number	n_{TC} parameter	$T_G^{¿}$ parameter
1	0.985	0.983
...	...	...
256	0.983	0.981
...	...	...
512	0.977	0.975
...	...	...
768	0.981	0.983
...	...	...
1024	0.982	0.987
...	...	...
1280	0.986	0.989

Table 3
Results of the training dataset homogeneity assessing according to the Fisher-Pearson and Fisher-Snedecor criterions

Parameter	The χ^2 calculated value / The $\chi^2(\alpha, 1)$ critical value	The F_{ij} calculated value / The $F_{critical}(\alpha = 0.01, 1279)$ critical value	Decision on the training dataset homogeneity
n_{TC}	6.418 / 6.6	1.122 /1.139	The dataset is homogeneity.
$T_G^{¿}$	6.476 / 6.6	1.128 /1.139	

To check the training dataset (Table 2) representativeness, the cluster analysis method (k-means [48]) was used. The training and test datasets were formed by random division. The proportion was 2:1, which is 67 and 33 % (858 and 422 elements, respectively). The training dataset's (Table 2)

clustering revealed 8 groups (classes I...VIII). This indicates the eight clusters identification. This observation confirms the training and test datasets (Figure 9) structure's similarity. Based on these results, the optimal dataset sizes for the n_{TC} and T_G^{i} parameters values were established. The training dataset consisted of 1280 elements (100 %). The control dataset consisted of 858 elements (67% of the training dataset). The test dataset consisted of 422 elements (33% of the training dataset).

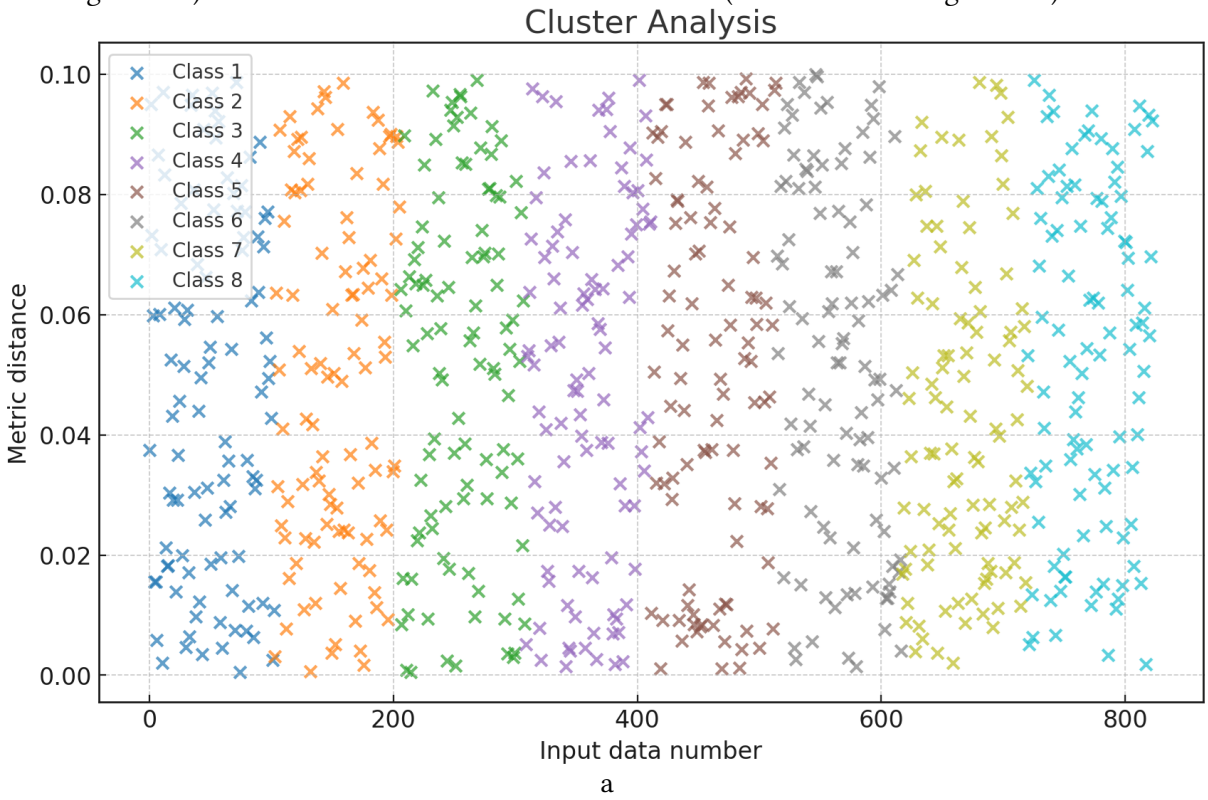

a

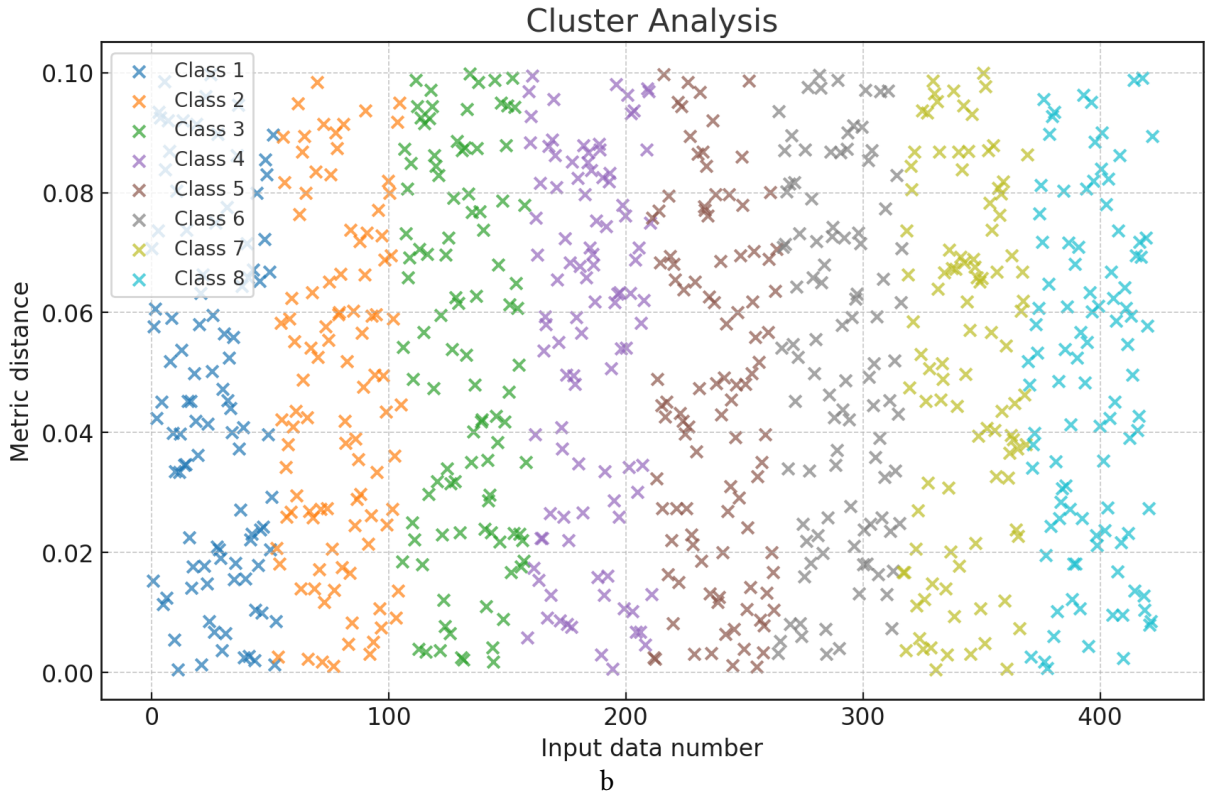

b

Figure 9: The parameters n_{TC} and T_G^{i} values cluster analysis results: (a) training dataset (858 elements); (b) test dataset (433 elements)

The proposed fully connected neural network (see Figure 2), consisting of two hidden layers with 16 and 8 neurons, respectively, was trained using the Keras library [49]. The "time_delay" factor was

separately allocated for the predict, and the original dataset was divided into training and test datasets, where the test dataset constituted 33 % of the total amount. SmoothReLU [35] was chosen as the activation function for the hidden layers, and the mean square error (MSE) [35] was used as the optimization criterion. The model was optimized using the Adam algorithm with the training step parameter set as 10^i, where i varies from 1 to 4. Each configuration was trained for 10 epochs, after which the most successful one was selected based on the loss function and predict accuracy indicators, which was then further trained for 100 epochs. The best results were demonstrated by the model configured with the Adam optimizer (training rate 0.0001) and two hidden layers containing 460 and 230 neurons, with SmoothReLU activation [35].

Figures 10 and 11 show the neural network's accuracy and loss diagrams. The obtained diagrams prove the neural network's convergence on 100 training epochs, since both the accuracy and loss on the training and test datasets coincide on the 100th training epoch. In this case, the accuracy reaches 0.99537 (99.537 %), and the loss decreases to 0.00511 (0.511 %). It is noted that after the 100th training epoch, the neural network's occurs overtraining effect. The neural network's overfitting effect, observed after 100 training epochs, is that the model begins to adjust too precisely to the training dataset, including its noise and random deviations, instead of identifying general patterns, which result the data on the training dataset continues to demonstrate high accuracy and low loss, and on the test (validation) set, a deterioration in performance is observed, since the model loses the ability to generalize to new data, having begun to "remember" the training dataset's specific features, which reduces its practical applicability.

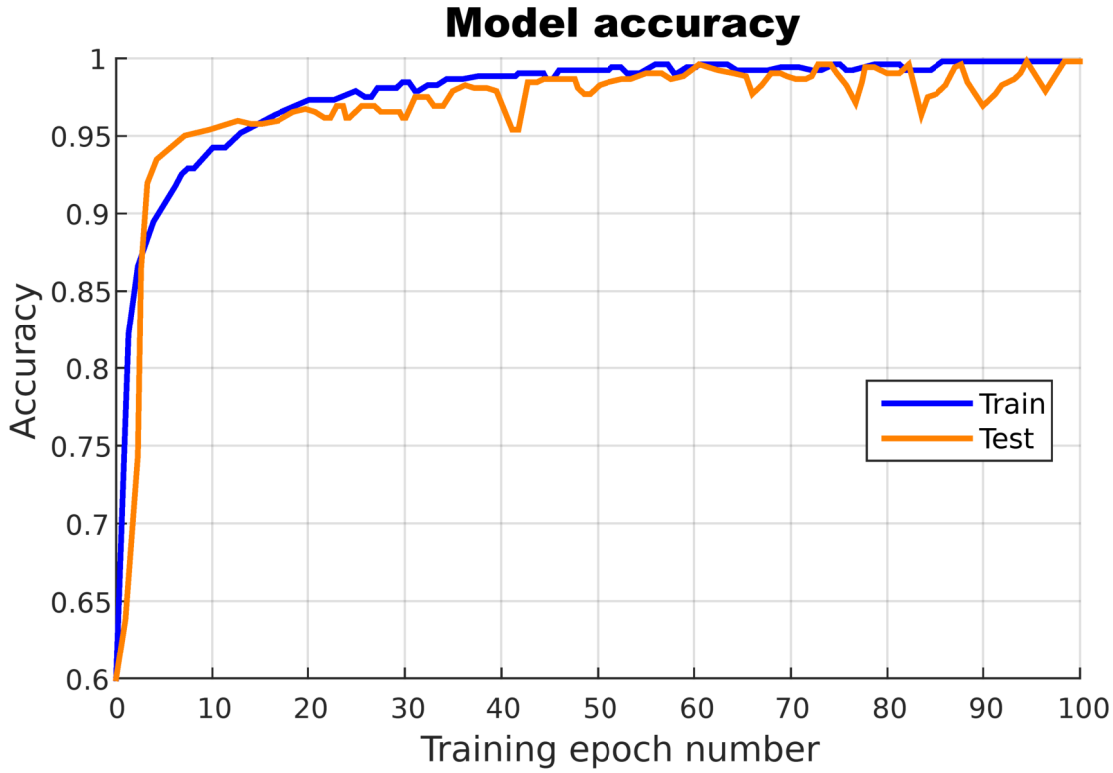

Figure 10: The developed neural network's accuracy metric diagram

Thus, it was found that further training leads to the neural network's generalization abilities deterioration. To prevent this effect, early stopping [50, 51] and regularization $\lambda \cdot \sum_{l=1}^{L} \left(W^{(l)}\right)_2^2$ in (33) were applied.

The developed neural network's predictive assessment ability was carried out on a test dataset, where Figure 12 shows a diagram demonstrating the delay value's predicted results correspondence to the actual data.

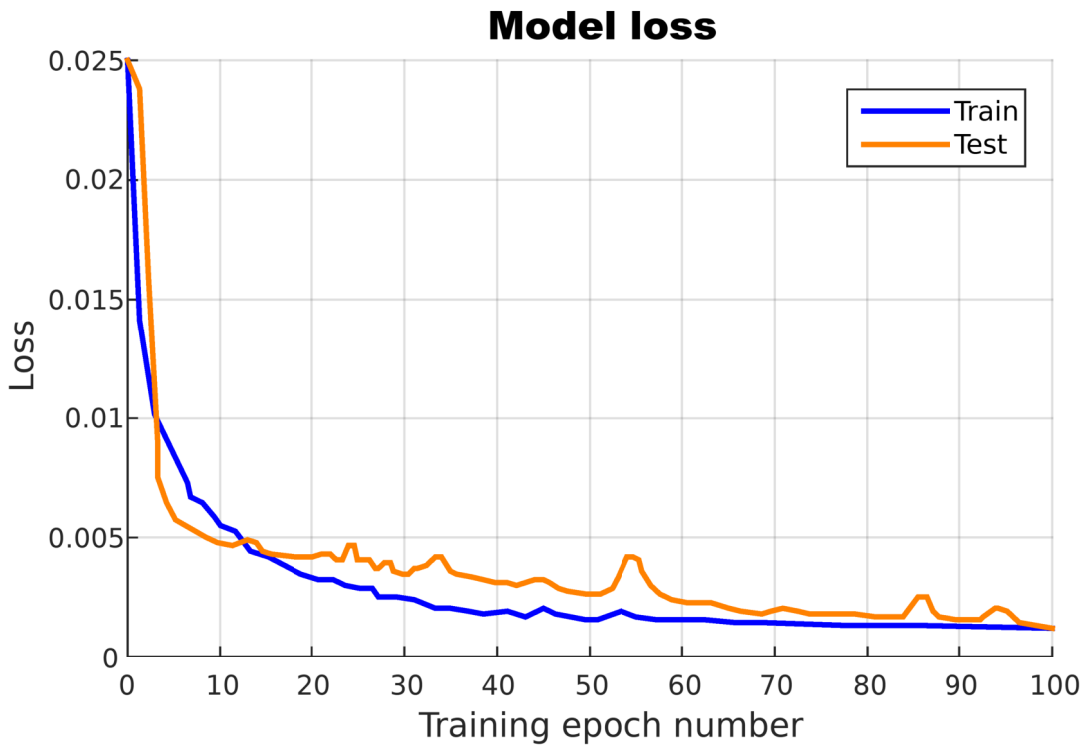

Figure 11: The developed neural network's loss function diagram

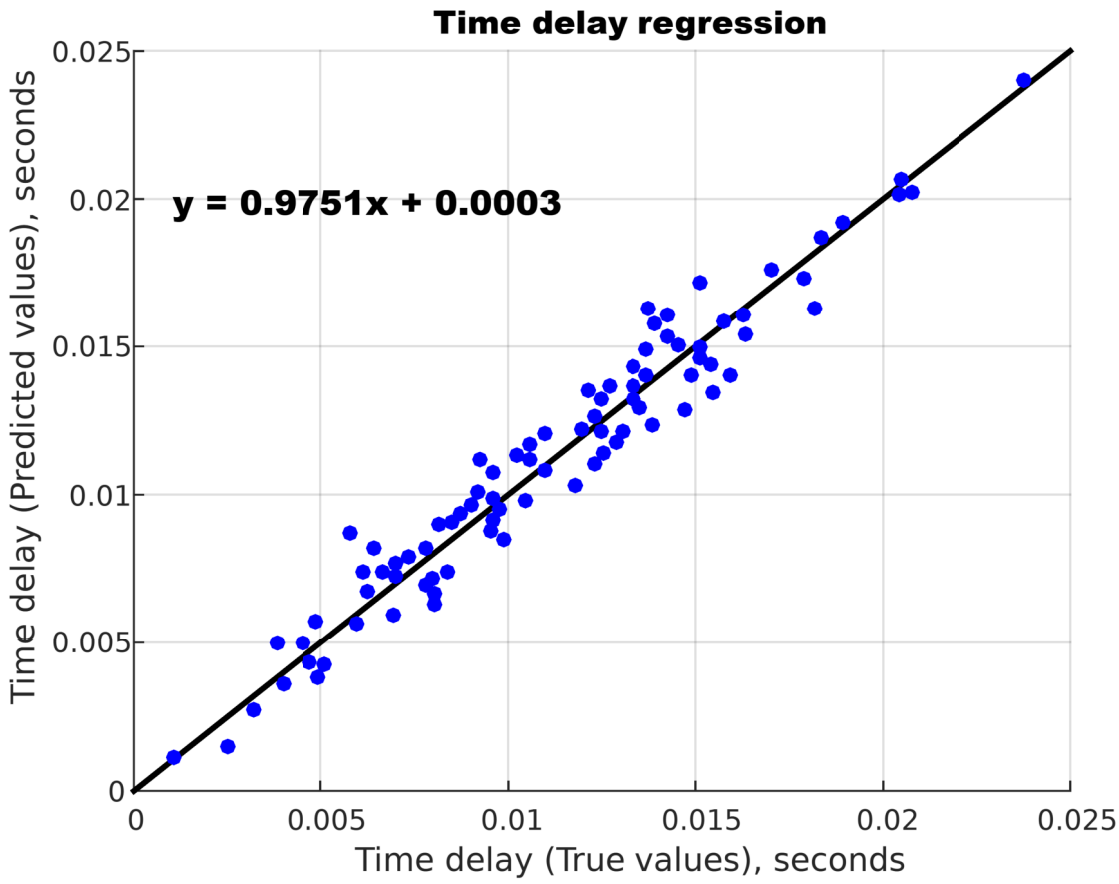

Figure 12: Diagram of predicted delay values vs. reference values

The predict errors distribution's analysis was also conducted, presented in Figure 13. It follows from the diagram that the developed model demonstrates high accuracy in determining delays in the gas temperature control channel based on the factor's given set, without an error's obvious bias in any direction.

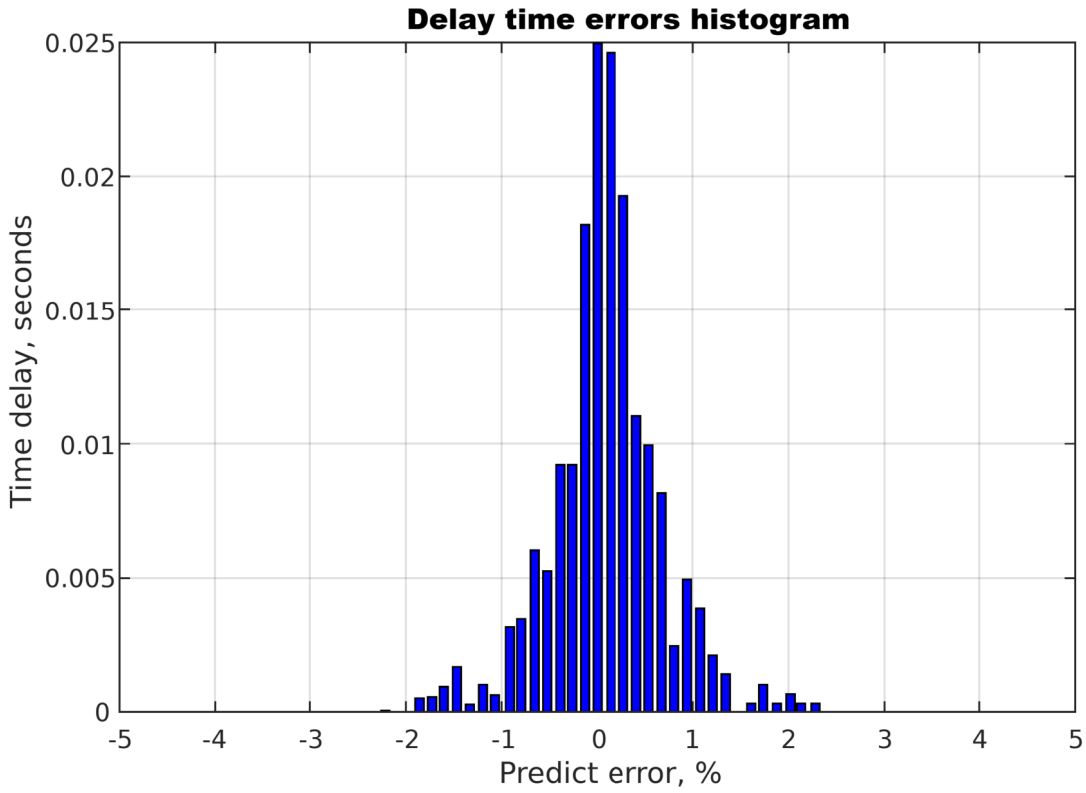

Figure 13: The predicted delay value's deviations distribution histogram

To assess the predicted delay values with the observed data correspondence, the determination coefficient and its adjusted version were calculated [52]. The obtained results R^2 = 0.9717 and adjusted R^2 = 0.9720 indicate a significant degree of relations between the neural network's predicts and the reference data.

To improve the predicted value's accuracy, a confidence interval construction technique is used, which aim is to take into account uncertainties arising from errors in data collection, errors in reference values, or random noise generated by a neural network with a reliability given level. Since there is no strictly mathematically sound algorithm for determining such intervals for neural networks, a quantile approach is proposed: the interval boundaries for the 95% reliability level [53] are set based on the quantiles of 0.025 and 0.975, which leads to the interval [−1.162; 1.077], covering forecast errors in 95% of the model cases (Figure 14).

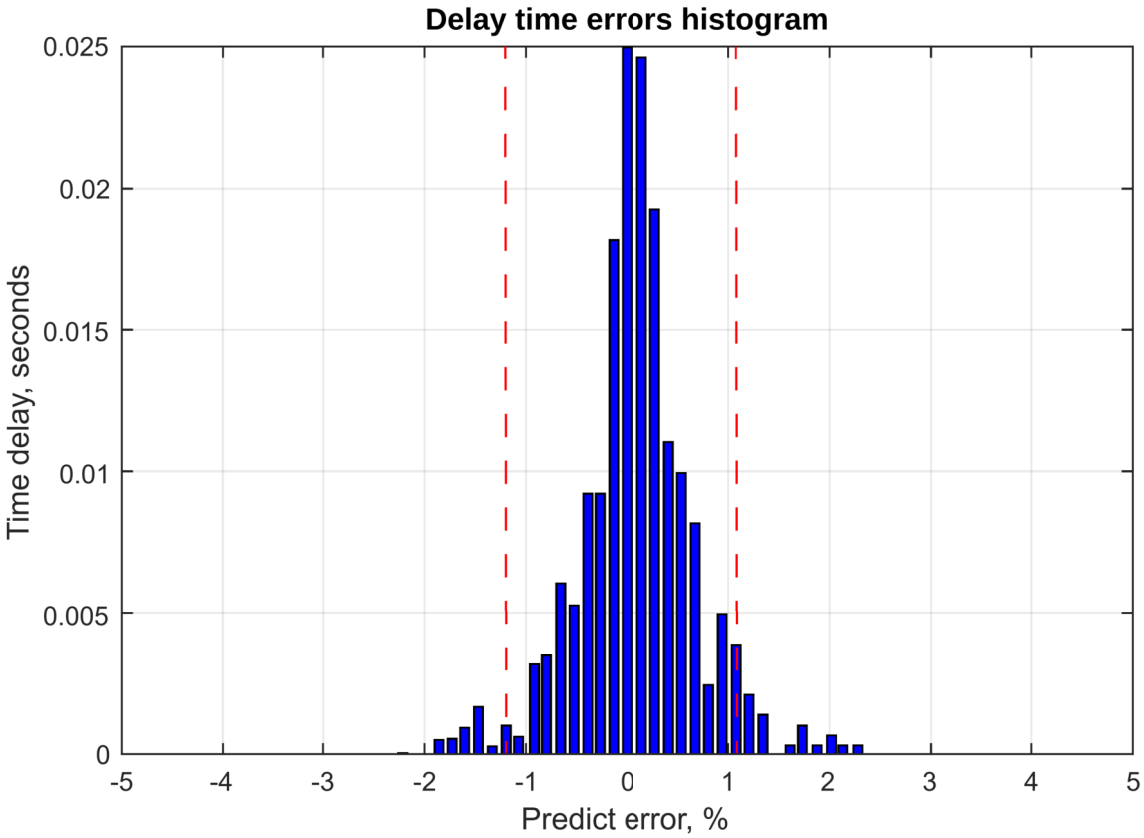

Figure 14: The predicted delay value's deviations distribution histogram with 95% interval of predicted value's deviations

Considering that 95 % of the neural network errors fall within this interval, we can conclude that for any predicted value of τ the following confidence interval is valid: $[\tau - 1.162; \tau + 1.077]$.

Figure 15 shows the dependence of the delay values on the frequency in the range from 1.9 to 2.1 Hz, with special attention paid to the 1.96 Hz point, where pronounced oscillations are recorded, which may indicate the system's resonance effects or specific dynamic features. The neural network use in this context has a positive effect on reducing the delay, since it is able to model complex nonlinear relations between system parameters and accurately predict optimal control modes, which ensures the control signal's timely correction. Due to the neural network's adaptability, it is possible to achieve a faster system response (the delay values using the neural network did not exceed 0.016 seconds, which is 36 % higher compared to the case without using a neural network), the operation stabilization in critical frequency ranges and, as a result, a significant reduction in delay.

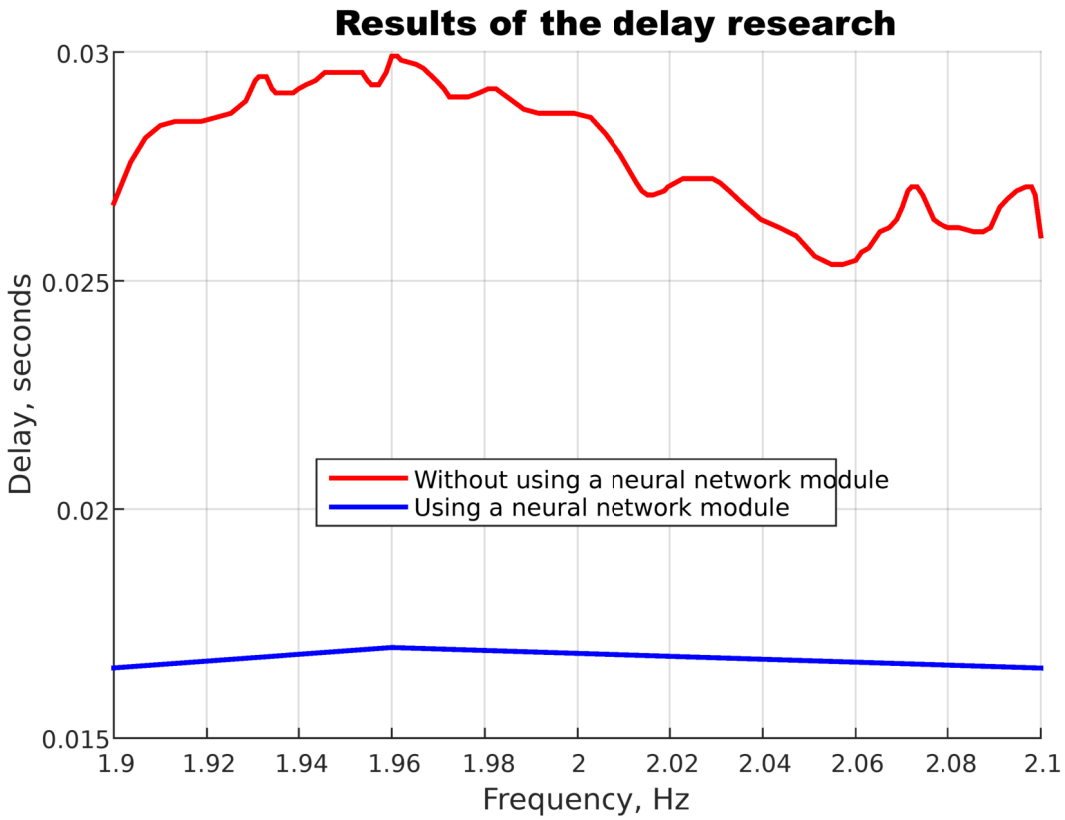

Figure 15: Diagram of the delay value's dynamics in the resonant frequency vicinity

6. Discussion

In this research, the helicopter TE's intelligent gas temperature controller (see Figure 1) was developed based on a double summation scheme, which allows for the measuring sensors inertial delays compensation and transient processes optimization in real time. Its special feature is the integration of adaptive algorithms with a differentiator and a neural network module, providing dynamic correction of control parameters and high control accuracy (up to 99.5 %).

A method has been developed based on a mathematical model of delayed dynamics (1) and determination of the control error (2), where the state is predicted using Taylor series expansion (6). The intelligent control law (8), supplemented by the coefficient's adaptive correction using the gradient descent scheme (9), allows real-time optimization of control parameters and compensation for inertial delays.

A neural network module for delay estimation correction (see Figure 2) has been developed, which is implemented using a deep fully connected neural network, which architecture is specified by (28)–(32), where the final delay estimation is determined according to (32). The module's special feature is the nonlinear activation functions use in hidden layers for accurate approximation of the relations between input features and delay correction, which ensures the system's dynamic adaptation in real time.

The neural network module's testing results demonstrate high training accuracy: the accuracy and loss function diagrams (Figures 10 and 11) confirm the model's convergence on the training and test datasets, and the predicted and reference delay value's correspondence diagram (Figure 12) indicates small predicting errors, which is further confirmed by the errors distribution on the histogram (Figure 13). In addition, the delay value's dynamics analysis in the resonant frequency vicinity (Figure 15) shows a 36 % reduction in delay, which indicates a significant improvement in the system's adaptive capabilities.

However, despite the positive dynamics and results achieved, the research has some limitations:

1. The modeling and testing results were obtained on the experimental data limited set basis (Figures 7 and 8), which may reduce the methodology applicability in conditions other than the test dataset.

2. The neural network module's overtraining effect is observed (Figures 10 and 11), which limits its ability to generalize and may negatively affect the delay prediction in real operating conditions.
3. The approximate compensation methods use, such as Taylor series expansion (6) and transfer function's simplification, may not provide sufficient accuracy of compensation for inertial delays during sudden changes in operating modes (Figure 15).

Future research could be structured as follows (Table 4).

Table 4
The future research roadmap

Number	Research direction	Action
1	Expansion of the experimental base and testing conditions	1. Conducting additional tests in various operating modes and extreme conditions to increase the data representativeness [54]. 2. Integrating data from various helicopter platforms and the experimental dataset's long-term collection to the specific conditions influence reduce [55].
2	The neural network module's stability and generalizing ability	1. The regularization method's design and implementation, ensemble models, and advanced architectures (e.g., RNNs or transformers) to prevent overfitting [56]. 2. Application of adaptive early stopping and cross-validation algorithms to improve of latency prediction's reliability [57].
3	Refining mathematical models for compensating inertial delays	1. The approximate methods extension (e.g., using more complex expansions or alternative dynamic models) to improve compensation accuracy, especially with sudden changes in operating modes [58]. 2. The adaptive self-tuning algorithms integration that allows the transfer function parameter's dynamic adjustment in real time [59].

The research demonstrates that the innovative adaptive control methods development requires technological improvements while simultaneously complying with regulatory and ethical standards when applying it on board a helicopter, taking into account the rights and responsibilities of human operators [60].

7. Conclusions

The helicopter TE's intelligent temperature controller has been developed that uses a double summation scheme with an adaptive observer and correction links, which provides effective compensation for the measuring sensor's inertial delays.

The neural network module's implementation for delay estimation correction allows the control parameter's dynamic adaptation in real time, which is a significant improvement compared to traditional approaches.

Simulation showed a reduction in overshoot from 8.0 to 1.5 % and a reduction in the transient process time from 4.2 to 3.3 seconds, and the neural network module's testing demonstrated a forecasting accuracy of 99.537 % (losses is 0.511 %) with a determination coefficient of R^2 = 0.9717 and a reduction in delay to 0.016 seconds (an improvement of 36 %).

In the future, authors are going to explore the experimental base and testing conditions expansion, including additional tests in various operating modes [61] and the data integration [62] from various helicopter platforms to reduce the specific conditions influence. They also plan to develop robust neural network modules using regularization methods [62], ensemble models [63], and adaptive algorithms [64], as well as refine the mathematical models for compensating for inertial delays by integrating adaptive self-tuning algorithms [65, 66] in real time.

Acknowledgements

The research was carried out with the support of the research projects "Theoretical and Applied Aspects of Development of the Aviation Sphere" of the Ministry of Internal Affairs of Ukraine (number 0123U104884) and "Information system development for automatic detection of misinformation sources and inauthentic behaviour of chat users" (number 187/0012 from 1/08/2024, 2023.04/0012).

Declaration on Generative AI

During the preparation of this work, the authors used Grammarly in order to: Grammar and spelling check. After using this tool, the authors reviewed and edited the content as needed and take full responsibility for the publication's content.

References

[1] A. Aziz, E. S. Mad Sariff, I. Shamsudheen, R. Abd Jamil, M. A. U. A. Abu Zarim, The effect of emergency floatation system (EFS) on helicopter stability during ditching, Transportation Engineering 14 (2023) 100206. doi: 10.1145/1188913.1188915

[2] A. de Voogt, E. St. Amour, Safety of twin-engine helicopters: Risks and operational specificity, Safety Science 136 (2021) 105169. doi: 10.1016/j.ssci.2021.105169

[3] T. Castiglione, D. Perrone, J. Song, L. Strafella, A. Ficarella, S. Bova, Linear model of a turboshaft aero-engine including components degradation for control-oriented applications, Energies 16:6 (2023) 2634. doi: 10.3390/en16062634

[4] M. Pasieka, N. Grzesik, K. Kuźma, Simulation modeling of fuzzy logic controller for aircraft engines, International Journal of Computing 16:1 (2017) 27–33. doi: 10.47839/ijc.16.1.868

[5] M. Li, Y. Luo, L. Qu, L. Xie, B. Zhao, Influence of ring gear flexibility on the fatigue reliability of planetary gear systems in heavy helicopters, Mechanism and Machine Theory 191 (2024) 105520. doi: 10.1016/j.mechmachtheory.2023.105520

[6] S. Vladov, Y. Shmelov, R. Yakovliev, Modified Helicopters Turboshaft Engines Neural Network On-board Automatic Control System Using the Adaptive Control Method, CEUR Workshop Proceedings 3309 (2024) 205–224. URL: https://ceur-ws.org/Vol-3309/paper15.pdf

[7] O. Lytviak, V. Loginov, S. Komar, Y. Martseniuk, Self-Oscillations of The Free Turbine Speed in Testing Turboshaft Engine with Hydraulic Dynamometer, Aerospace 8:4 (2021) 114. doi: 10.3390/aerospace8040114

[8] H. Zhang, Z. Wang, F. Teng, P. Xia, Dynamic Strain Measurement of Rotor Blades in Helicopter Flight Using Fiber Bragg Grating Sensor, Sensors 23:15 (2023) 6692. doi: 10.3390/s23156692

[9] Z. Yu, X. Yan, R. Chen, Prediction of pilot workload in helicopter landing after one engine failure, Chinese Journal of Aeronautics 33:12 (2020) 3112–3124. doi: 10.1016/j.cja.2020.05.021

[10] P. Kurdel, A. Novák, A. N. Sedláčková, L. Korba, The Methods of Helicopter Control in Non-standard Situations, Transportation Research Procedia 59 (2021) 214–222. doi: 10.1016/j.trpro.2021.11.113

[11] Y. Wang, C. Ji, Z. Xi, H. Zhang, Q. Zhao, An adaptive matching control method of multiple turboshaft engines, Engineering Applications of Artificial Intelligence 123 (2023) 106496. 2023. doi: 10.1016/j.engappai.2023.106496

[12] Y. Shmelov, S. Vladov, Y. Klimova, M. Kirukhina, Expert system for identification of the technical state of the aircraft engine TV3-117 in flight modes. In Proceedings of the System Analysis & Intelligent Computing : IEEE First International Conference on System Analysis & Intelligent Computing (SAIC), 08–12 October 2018, pp. 77–82. doi: 10.1109/SAIC.2018.8516864

[13] S. Yepifanov, O. Bondarenko, Forming of turboshaft engine mathematical model, Aerospace Technic and Technology 4sup1 (2023) 85–94. doi: 10.32620/aktt.2023.4sup1.12

[14] Y. Wang, Q. Zheng, Z. Xu, H. Zhang, A novel control method for turboshaft engine with variable rotor speed based on the Ngdot estimator through LQG/LTR and rotor predicted torque feedforward, Chinese Journal of Aeronautics 33:7 (2020) 1867–1876. doi: 10.1016/j.cja.2020.01.009

[15] S. Yepifanov, O. Bondarenko, Development of Turboshaft Engine Adaptive Dynamic Model: Analysis of Estimation Errors, Transactions on Aerospace Research 2022:4 (2022) 59–71. doi: 10.2478/tar-2022-0024

[16] L. Jia, Z. Li, Y. Bai, J. Wu, L. Gao, Z. Chen, Design of the Turboshaft Engine Acceleration and Deceleration Control Schedules Based on Direct Simulation Method, in: Z. H. Zhu, X. Wei, R. Li (Eds.), Trends in Advanced Unmanned Aerial Systems. ICAUAS 2024, Springer Aerospace Technology. Springer, Singapore, 2025, pp. 269–277. doi: 10.1007/978-981-96-3240-4_29
[17] T.-D. Le, D. C. Nguyen, T. L. Nguyen, Analysing temperature distributions in turbine first-stage rotor blades of a helicopter turboshaft engine, Journal of Science and Transport Technology 4:3 (2024) 1–10. doi: 10.58845/jstt.utt.2024.en.4.3.1-10
[18] Y. Wang, C. Cai, J. Song, H. Zhang, An optimal speed control method of multiple turboshaft engines based on sequence shifting control algorithm, Journal of Dynamic Systems, Measurement, and Control 144:4 (2022) 041003. doi: 10.1115/1.4053088
[19] H. Mao, Y. Guo, R. Li, C. Lai, Versatile Simulation Platform for Turboshaft Engine Control System, In Proceedings of the 2019 Chinese Control Conference (CCC), Guangzhou, China, 27–30 July 2019, pp. 7211–7216, Jul. 2019. doi: 10.23919/ChiCC.2019.8865902
[20] Y. Wang, C. Ji, Z. Xi, H. Zhang, Q. Zhao, An adaptive matching control method of multiple turboshaft engines, Engineering Applications of Artificial Intelligence 123 (2023) 106496. doi: 10.1016/j.engappai.2023.106496
[21] D. Cheng, L. Liu, Z. Yu, A Nonlinear H∞ Set-point Control Method for Turbofan Engines with Disturbances. International Journal of Control, Automation and Systems 19 (2021) 3062–3074. doi: 10.1007/s12555-020-0436-3
[22] S. Tovkach, Middleware Service for the Integration of Control Systems of the Aviation Engine and Aircraft, in: A. Bieliatynskyi, V. Breskich, (eds), Safety in Aviation and Space Technologies. Lecture Notes in Mechanical Engineering. Springer, Cham. doi: 10.1007/978-3-030-85057-9_2
[23] S. Vladov, L. Scislo, V. Sokurenko, O. Muzychuk, V. Vysotska, A. Sachenko, A. Yurko, Helicopter Turboshaft Engines' Gas Generator Rotor R.P.M. Neuro-Fuzzy On-Board Controller Development, Energies, 17:16 (2024), 4033. doi: 10.3390/en17164033
[24] O. Balli, Exergetic, sustainability and environmental assessments of a turboshaft engine used on helicopter, Energy 276 (2023) 127593. doi: 10.1016/j.energy.2023.127593.
[25] I. Andrianov, A. Shatrov, Padé Approximants, Their Properties, and Applications to Hydrodynamic Problems, Symmetry 13:10 (2021) 1869. doi: 10.3390/sym13101869
[26] L. Dubchak, A. Sachenko, Y. Bodyanskiy, C. Wolff, N. Vasylkiv, R. Brukhanskyi, V. Kochan, Adaptive Neuro-Fuzzy System for Detection of Wind Turbine Blade Defects. Energies 17:24 (2024) 6456. doi: 10.3390/en17246456
[27] S. J. Mohammadi, S. A. M. Fashandi, S. Jafari, T. Nikolaidis, A scientometric analysis and critical review of gas turbine aero-engines control: From Whittle engine to more-electric propulsion, Measurement and control 54:5–6 (2021) 935–966, 2021. doi: 10.1177/0020294020956675
[28] M. Komar, A. Sachenko, V. Golovko, V. Dorosh, Compression of network traffic parameters for detecting cyber attacks based on deep learning. In Proceedings of the 2018 IEEE 9th International Conference on Dependable Systems, Services and Technologies (DESSERT), Kyiv, Ukraine, 2018, pp. 43–47. doi: 10.1109/DESSERT.2018.8409096
[29] N. Vasylkiv, L. Dubchak, I. Turchenko, I. Ivashchuk, R. Savchyshyn, Fuzzy Estimation Method of Information System Providing Part Influence on the Functioning Quality. In Proceedings of the 2019 10th IEEE International Conference on Intelligent Data Acquisition and Advanced Computing Systems: Technology and Applications (IDAACS), Metz, France, 2019, pp. 980–984. doi: 10.1109/IDAACS.2019.8924249
[30] I. Perova, Y. Bodyanskiy, Fast medical diagnostics using autoassociative neuro-fuzzy memory, International Journal of Computing 16:1 (2017) 34–40. doi: 10.47839/ijc.16.1.869.
[31] A. R. Marakhimov, K. K. Khudaybergenov, Approach to the synthesis of neural network structure during classification, International Journal of Computing 19:1 (2020) 20–26. doi: 10.47839/ijc.19.1.1689
[32] S. Vladov, Y. Shmelov, M. Petchenko. A Neuro-Fuzzy Expert System for the Control and Diagnostics of Helicopters Aircraft Engines Technical State, CEUR Workshop Proceedings 3013 (2021) 40–52. URL: https://ceur-ws.org/Vol-3013/20210040.pdf
[33] B. Rusyn, O. Lutsyk, R. Kosarevych, O. Kapshii, O. Karpin, T. Maksymyuk, J. Gazda, Rethinking Deep CNN Training: A Novel Approach for Quality-Aware Dataset Optimization, IEEE Access 12 (2024) 137427–137438. doi: 10.1109/access.2024.3414651
[34] G. R. Matuck, J. R. Barbosa, C. Bringhenti, I. Lima, Gas Turbine Fault Detection and Isolation Using MLP Artificial Neural Network, In Proceedings of the ASME Turbo Expo 2007: Power for

Land, Sea, and Air, Montreal, Canada, 14–17 May, 2007, vol. 1, pp. 803–811. doi: 10.1115/gt2007-27987
[35] S. Vladov, A. Sachenko, V. Sokurenko, O. Muzychuk, V. Vysotska, Helicopters Turboshaft Engines Neural Network Modeling under Sensor Failure, Journal of Sensor and Actuator Networks 13:5 (2024) 66. doi: 10.3390/jsan13050066
[36] N. Vasylkiv, I. Turchenko, L. Dubchak, "Fuzzy Model of the IT Project Environment Impact on its Completion. In Proceedings of the 2020 10th International Conference on Advanced Computer Information Technologies (ACIT), Deggendorf, Germany, 2020, pp. 302–305. doi: 10.1109/ACIT49673.2020.9208914
[37] I. Perova, Y. Bodyanskiy, Adaptive human machine interaction approach for feature selection-extraction task in medical data mining, International Journal of Computing 17:2 (2018) 113–119. doi: 10.47839/ijc.17.2.997
[38] S. Vladov, Y. Shmelov, R. Yakovliev, Helicopters Aircraft Engines Self-Organizing Neural Network Automatic Control System, CEUR Workshop Proceedings 3137 (2022) 28–47. doi: 10.32782/cmis/3137-3 URL: https://ceur-ws.org/Vol-3137/paper3.pdf
[39] S. Vladov, Y. Shmelov, R. Yakovliev, Y. Stushchankyi, Y. Havryliuk, Neural Network Method for Controlling the Helicopters Turboshaft Engines Free Turbine Speed at Flight Modes, CEUR Workshop Proceedings 3426 (2023) 89–108. URL: https://ceur-ws.org/Vol-3426/paper8.pdf
[40] S. Yepifanov, Aircraft Turbine Engine Automatic Control Based on Adaptive Dynamic Models, Transactions on Aerospace Research 2020:4 (2020) 61–70. doi: 10.2478/tar-2020-0021
[41] Y. Yin, X. Heng, H. Zhang, A. Wang, Modeling method and dynamic analysis of turboshaft engine combustor rotor with curvic couplings considering thermal contact resistance under temperature field influence, Results in Engineering 25 (2025) 103853. doi: 10.1016/j.rineng.2024.103853
[42] R. M. Catana, G. Dediu, Analytical Calculation Model of the TV3-117 Turboshaft Working Regimes Based on Experimental Data, Applied Sciences 13:19 (2023) 10720. doi: 10.3390/app131910720
[43] V. Lytvyn, D. Dudyk, I. Peleshchak, R. Peleshchak, P. Pukach, Influence of the Number of Neighbours on the Clustering Metric by Oscillatory Chaotic Neural Network with Dipole Synaptic Connections, CEUR Workshop Proceedings 3664 (2024) 24–34. URL: https://ceur-ws.org/Vol-3664/paper3.pdf
[44] H.-Y. Kim, Statistical notes for clinical researchers: Chi-squared test and Fisher's exact test, Restorative Dentistry & Endodontics 42:2 (2017) 152. doi: 10.5395/rde.2017.42.2.152
[45] Z. Hu, E. Kashyap, O. K. Tyshchenko, GEOCLUS: A Fuzzy-Based Learning Algorithm for Clustering Expression Datasets, Lecture Notes on Data Engineering and Communications Technologies 134 (2022) 337–349. doi: 10.1007/978-3-031-04812-8_29
[46] C. M. Stefanovic, A. G. Armada, X. Costa-Perez, Second Order Statistics of Fisher-Snedecor Distribution and Their Application to Burst Error Rate Analysis of Multi-Hop Communications, IEEE Open Journal of the Communications Society 3 (2022) 2407–2424. doi: 10.1109/ojcoms.2022.3224835
[47] M. Komar, V. Golovko, A. Sachenko, S. Bezobrazov, Development of neural network immune detectors for computer attacks recognition and classification. In Proceedings of the 2013 IEEE 7th International Conference on Intelligent Data Acquisition and Advanced Computing Systems (IDAACS), Berlin, Germany, 2013, pp. 665–668. doi: 10.1109/IDAACS.2013.6663008
[48] S. Babichev, J. Krejci, J. Bicanek, V. Lytvynenko, Gene expression sequences clustering based on the internal and external clustering quality criteria. In Proceedings of the 2017 12th International Scientific and Technical Conference on Computer Sciences and Information Technologies (CSIT), Lviv, Ukraine, 05–08 September 2017. doi: 10.1109/STC-CSIT.2017.8098744
[49] N. Shakhovska, V. Yakovyna, N. Kryvinska, An improved software defect prediction algorithm using self-organizing maps combined with hierarchical clustering and data preprocessing. Lecture Notes in Computer Science 12391 (2020) 414–424. doi: 10.1007/978-3-030-59003-1_27
[50] V. Turchenko, E. Chalmers, A. Luczak, A deep convolutional auto-encoder with pooling – unpooling layers in caffe, International Journal of Computing 18:1 (2019) 8–31. doi: 10.47839/ijc.18.1.1270
[51] V. V. Morozov, O. V. Kalnichenko, O. O. Mezentseva, The method of interaction modeling on basis of deep learning the neural networks in complex IT-projects, International Journal of Computing 19:1 (2020) 88–96. doi: 10.47839/ijc.19.1.1697
[52] A. Berko, V. Alieksieiev, V. Holdovanskyi, Determination-based correlation coefficient, CEUR Workshop Proceedings 3711 (2024) 198–224. URL: https://ceur-ws.org/Vol-3711/paper12.pdf

[53] N. Shakhovska, V. Yakovyna, Feature Selection and Software Defect Prediction by Different Ensemble Classifiers, Lecture Notes in Computer Science 12923 (2021) 307–313. doi: 10.1007/978-3-030-86472-9_28
[54] J. Rabcan, V. Levashenko, E. Zaitseva, M. Kvassay, S. Subbotin, Non-destructive diagnostic of aircraft engine blades by Fuzzy Decision Tree, Engineering Structures 197 (2019 109396. doi: 10.1016/j.engstruct.2019.109396
[55] U. Ahmed, A. Fakhre, I. Jennions, A review of aircraft auxiliary power unit faults, diagnostics and acoustic measurements, Progress in Aerospace Sciences 124 (2021) 100721. doi: 10.1016/j.paerosci.2021.100721
[56] Y. V. Bodyanskiy, O. K. Tyshchenko, A Hybrid Cascade Neuro–Fuzzy Network with Pools of Extended Neo–Fuzzy Neurons and Its Deep Learning, International Journal of Applied Mathematics and Computer Science 29:3 (2019) 477–488. doi: 10.2478/amcs-2019-0035
[57] V. Kovtun, T. Altameem, M. Al-Maitah, W. Kempa, Entropy-Metric Estimation of the Small Data Models with Stochastic Parameters, Heliyon 10 (2024) e24708. doi: 10.1016/j.heliyon.2024.e24708
[58] J. Rabcan, V. Levashenko, E. Zaitseva, M. Kvassay, S. Subbotin, Application of Fuzzy Decision Tree for Signal Classification, IEEE Transactions on Industrial Informatics 15:10 (2019) 5425–5434, Oct. 2019. doi: 10.1109/tii.2019.2904845
[59] S. Leoshchenko, A. Oliinyk, S. Subbotin, M. Ilyashenko, T. Kolpakova, Neuroevolution methods for organizing the search for anomalies in time series, CEUR Workshop Proceedings 3392 (2023) 164–176. URL: https://ceur-ws.org/Vol-3392/paper14.pdf
[60] S. Ablamskyi, O. Muzychuk, E. D'Orio, and V. Romaniuk, Taking biological samples from a person for examination in criminal proceedings: correlation between obtaining evidence and observing human rights, Revista de Direito Internacional 20:1 (2023). doi: 10.5102/rdi.v20i1.8859
[61] A. Sachenko, V. Kochan, R. Kochan, V. Turchenko, K. Tsahouridis, T. Laopoulos, Error compensation in an intelligent sensing instrumentation system. In IMTC 2001. Proceedings of the 18th IEEE Instrumentation and Measurement Technology Conference. Rediscovering Measurement in the Age of Informatics (Cat. No.01CH 37188), Budapest, Hungary, 2001, vol. 2, pp. 869–874. doi: 10.1109/IMTC.2001.928201
[62] A. Sachenko, V. Kochan, V. Turchenko, Intelligent distributed sensor network. In Proceedings of the IMTC/98 Conference Proceedings. IEEE Instrumentation and Measurement Technology Conference. Where Instrumentation is Going (Cat. No.98CH36222), St. Paul, MN, USA, 1998, vol. 1, pp. 60–66. doi: 10.1109/IMTC.1998.679663
[63] C. Wang, N. Shakhovska, A. Sachenko, M. Komar, A New Approach for Missing Data Imputation in Big Data Interface. Information Technology and Control 49:4 (2020) 541–555. doi: 10.5755/j01.itc.49.4.27386
[64] A. Urooj, S. Elferik, Adaptive Particle Swarm Optimization based Self-Tuning Control for Combustion Engines. Transportation Research Procedia 84 (2025) 97–104. doi: 10.1016/j.trpro.2025.03.051
[65] D. von Eschwege, A. Engelbrecht, Soft Actor-Critic Approach to Self-Adaptive Particle Swarm Optimisation, Mathematics 12:22 (2024) 3481. doi: 10.3390/math12223481.
[66] S. Arof, E. Noorsal, S. Z. Yahaya, Z. Hussain, Y. Mohd Ali, M. H. Abdullah, M. K. Safie, Adaptive Sliding Mode Feedback Control Algorithm for a Nonlinear Knee Extension Model. Machines 11:7 (2023) 732. doi: 10.3390/machines11070732.